Stratigraphy and provenance of the Paleogene syn-rift sediments in central-southern Palawan: Paleogeographic significance for the South China margin

Wen-Huang Chen[1, 2, 3, 4], Yi Yan[1, 3*], Andrew Carter[5], Chi-Yue Huang[6], Graciano P. Yumul Jr.[7], Carla B. Dimalanta[8], Jillian Aira S. Gabo-Ratio[8], Ming-Huei Wang[9], Duofu Chen[10], Yehua Shan[1], Xin-Chang Zhang[1], and Weiliang Liu[11]

[1]Key Laboratory of Ocean and Marginal Sea Geology, Guangzhou Institute of Geochemistry, Chinese Academy of Sciences, Guangzhou 510640, China
[2]Southern Marine Science and Engineering Guangdong Laboratory (Guangzhou), Guangzhou 511458, China
[3]Innovation Academy of South China Sea Ecology and Environmental Engineering, Chinese Academy of Sciences, Guangzhou, 510640, China
[4]Guangdong Provincial Key Laboratory of Marine Resources and Coastal Engineering, Guangzhou 510006, China
[5]Department of Earth and Planetary Sciences, Birkbeck, University of London, Malet Street, London WC1E 7HX, United Kingdom
[6]School of Ocean and Earth Science, Tongji University, Shanghai 200092, China
[7]Cordillera Exploration Company Incorporated, NAC Tower, Bonifacio Global City, Taguig, Metro Manila 1634, Philippines
[8]Rushurgent Working Group–Tectonics and Geodynamics Academic Group, National Institute of Geological Sciences, College of Science, University of the Philippines Diliman, Quezon City 1101, Philippines
[9]Exploration and Development Research Institute, CPC Corporation, Taiwan, Miaoli 36042, Taiwan
[10]Shanghai Engineering Research Center of Hadal Science and Technology, College of Marine Sciences, Shanghai Ocean University, Shanghai 201306, China
[11]School of Marine Sciences, Sun Yat-Sen University, Guangzhou 510006, China

*Corresponding Author: Yi Yan, yanyi@gig.ac.cn

Key Points:

- Age of breakup unconformity of Palawan microcontinent block (33–32 Ma) demonstrate its conjugate relationship with Pearl River Mouth Basin

- Both interior Cathaysia block and local basement uplifts supplied syn-rift sediments to central-southern Palawan on the continental slope
- Sediment routing on the South China margin imply a wide rifted margin with very low topographic gradient before seafloor spreading

Abstract

The Palawan microcontinental block is thought to have separated from the South China margin due to seafloor spreading and opening of the South China Sea. However, it is uncertain when and from which section the Palawan microcontinental block rifted from the South China margin, and little is known about sediment routing across the rifted margin before continental breakup. To address these aspects we studied the biostratigraphy and provenance of syn-rift sedimentary rocks collected from the Panas-Pandian Formation in central-southern Palawan. Micropaleontological evidence indicates a Middle Eocene–earliest Oligocene (47.7–32.9 Ma) age for the Panas-Pandian Formation. Based on this and the oldest age of the post-rift Nido Limestone (~32 Ma), the breakup unconformity on the Palawan microcontinent block is dated around 33–32 Ma. This timing of breakup unconformity is close to that of the Pearl River Mouth Basin (~30 Ma) and IODP Site U1435 (~34Ma), suggesting the conjugate relationship between the Palawan microcontinental block and the Pearl River Mouth Basin. Trace fossils and benthic foraminifera from the Panas-Pandian Formation indicate a middle bathyal to abyssal environment on the continental slope of the South China margin. Multidisciplinary provenance analysis reveals that the Panas-Pandian Formation was derived from both local Mesozoic basement uplifts and the interior Cathaysia Block. It indicates that a paleo-Pearl River has been established at least since the Middle Eocene (47.7– 42.1 Ma) and could deliver sediments from the interior Cathaysia Block to the continental slope, across the wide rifted margin with a low topographic gradient.

1. Introduction

Microcontinents preserve records of continental rifting and breakup, seafloor spreading and microcontinent accretion, and thus provide insights into the paleogeography and evolution of continental margins (e.g. Borissova et al., 2003; Carter et al., 2014; Waldron & van Staal, 2001). The South China Sea (SCS) is one of the largest marginal seas in the western Pacific (Figure 1) that ruptured during the late Eocene with seafloor spreading spanning the Early Oligocene–Middle Miocene (~33–16 Ma), following rifting and thinning

of the continental lithosphere which dates back to the Latest Cretaceous, (e.g. Barckhausen et al., 2014; Briais et al., 1993; Li et al., 2014; Taylor & Hayes, 1983). Ocean spreading led to the formation of conjugate continental margins (Figure 1). Of these the northern margin has seen most study (e.g. Li et al., 2014, 2015; Sun et al., 2018; Wang et al., 2000, 2012), to the extent that relatively little is known about the formation and development of the southeastern margin represented by the Palawan microcontinental block (e.g. Yumul et al., 2003). The Palawan microcontinental block spans the area of Palawan, Mindoro, western Panay and the Romblon Islands, in the southwest Philippines, and the Reed Bank (Figure 1) (Hinz & Schlüter, 1985; Holloway, 1982; Liu et al., 2014; Yumul et al., 2009). Palawan is commonly thought to be a continental fragment that rifted and drifted away from mainland China during seafloor spreading of the SCS helped by the southward subduction of the Proto-SCS beneath the Cagayan Ridge. (Holloway, 1982; Taylor & Hayes, 1983; Yumul et al., 2003, 2009). The geology of Palawan, especially, the Eocene-Oligocene, is therefore key to understanding the early stages of rifting and the paleogeography of the South China margin, prior to opening of the SCS.

The Palawan microcontinental block is located east of the Dangerous Grounds and west of the Philippines Mobile Belt (Figure 1). Seismostratigraphy offshore the northwestern Palawan shelf (Franke et al. 2011) has identified four tectonostratigraphic units: (1) Mesozoic pre-rift metasediments/sediments associated with an active margin; (2) Latest Cretaceous–Eocene syn-rift sediments associated with rifting; (3) Oligocene–Early Miocene post-rift sediments concurrent with the drifting of Palawan; and (4) Late Miocene–Recent sediments formed during and after collision between Palawan and the Cagayan Ridge-Philippine Mobile Belt. Due to this collision, Paleogene syn-rift sediments, known as the Panas-Pandian Formation, that were originally deposited on the southern continental margin were thrusted, uplifted and juxtaposed with ophiolites as seen in central-southern Palawan (Aurelio et al., 2014) (Figure 2b). As a sedimentary archive of the early stages of continental breakup, the Panas-Pandian Formation is a good place to study the paleogeography of the South China margin prior to opening of the SCS.

Whilst the provenance of syn-rift sediments have been used to argue for a connection between the Palawan microcontinental block and the northern SCS margin (Concepcion et al., 2012; Shao, Cao, et al., 2017; Yan et al., 2018), the lack of direct stratigraphic evidence means that it is unknown when and where exactly the Palawan microcontinental block rifted from the South China margin. A useful indicator would be a similar timing of the breakup unconformity since along the South China continental margin it follows the stepwise

propagation of seafloor spreading from northeast to southwest (Franke, 2013; Morley, 2016). Currently the breakup unconformity along the northern margin of the Palawan microcontinental block is poorly constrained because few boreholes have been drilled into the syn-rift sediments. As a consequence age constraints have depended on the age of post-rift platform carbonates (Nido Limestone) (Franke, 2013). Syn-rift sediments exposed on central-southern Palawan (Panas-Pandian Formation) are mostly unmetamorphosed and contain fine-grained sediments, and are thus suitable for biostratigraphic study to better constrain the age of the breakup unconformity. Improved age control would help define which section of the south China margin Palawan came from.

Until recently, little has been known about the origin and routing of syn-rift sediments deposited across the rifted South China margin. As the development of half-grabens and grabens are generally accompanied by uplift and erosion of horst blocks, it is reasonable to expect the dominance of a proximal sources for the syn-rift sediments as widely demonstrated for Eocene syn-rift sediments from the Pearl River Mouth Basin (Shao et al., 2016; Wang et al., 2017) and at International Ocean Discovery Program (IODP) Site U1435 (Shao, Meng, et al., 2017). Sediments sourced from the interior of continental South China with a Cathaysian affinity, potentially delivered by a paleo-Pearl River like its present-day northeastern tributaries (the Bei and Dong Rivers) have been detected in late Early Oligocene rocks from boreholes X28 and P33 in the Pearl River Mouth Basin (Cao et al., 2018; Shao et al., 2016; Wang et al., 2019) (Figure 1). Potentially, these sediments may have reached the Palawan sector of the continental margin prior to it drifting away but this would depend on the geomorphology of the rifted continental margin, such as whether a narrow, elongate deep-sea basin/gulf existed (Li et al., 2017; Wang et al., 2003). As a consequence a provenance study of the Paleogene Panas-Pandian Formation will help improve understanding of margin development and sediment routing across the South China margin prior to breakup.

To address these aspects, our study examined the biostratigraphy and provenance of syn-rift sedimentary rocks collected from the Panas-Pandian Formation in central-southern Palawan. Specifically, we determined the deposition age of the Panas-Pandian Formation using new planktonic foraminifers and calcareous nannofossil data together with the biostratigraphic results of Wolfart et al. (1986). This new age helps to constrain the timing of the breakup unconformity on the Palawan microcontinental block and therefore helps to elucidate its conjugate relationship with the northern SCS margin. Benthic foraminiferal and sedimentological evidence are used to reconstruct the depositional environment. To constrain sediment provenance and routing we adopted a multidisciplinary approach using trace

elements, Nd isotope, heavy mineral assemblages and detrital zircon U-Pb geochronology (in combination with previously published detrital results).

2. Geologic Setting

2.1. The South China margin

The continental margin of South China has experienced a complex tectonic evolution. It was an Andean-type active margin between the Permian and mid-Cretaceous, and then evolved to a western Pacific-type margin in the Late Cretaceous (Li et al., 2012). The margin finally became a passive margin in the Cenozoic owing to extension and rifting followed by opening of the SCS. The South China continent is conventionally divided into the Yangtze Block in the northwest and the Cathaysia Block in the southeast, along the Jiangshao Fault Zone (Figure 1). The Cathaysia Block has a basement dominated by Paleoproterozoic to Neoproterozoic (2500–540 Ma) units with minor Archean (3500–2500 Ma) components, overlain by the Paleozoic and Mesozoic sedimentary strata (Chen & Jahn, 1998; Xu et al., 2007; Yu et al., 2006). A series of magmatic events, i.e. Caledonian (570–400 Ma), Indosinian (257–205 Ma) and Yanshannian (180–67 Ma) have taken place within the Cathaysia Block since the Paleozoic. Caledonian and Indosinian granitoids are mainly distributed along the northern boundary of the Cathaysia Block and the interior of the Yangtze Block (Chen & Jahn, 1998). Mesozoic (Yanshanian) granitoids are however extensively exposed on the Cathaysia Bock as well as the northern SCS continental margin (Chen & Jahn, 1998; Li et al., 2018; Ye et al., 2018) and fall into two age groups: Jurassic (Early Yanshanian) and Cretaceous (Late Yanshanian). These Jurassic-Cretaceous rocks generally show an oceanward younging trend as a result of steepening of the subduction angle of the Pacific Plate beneath Eurasia (Li & Li, 2007). The Taixinan Basin, Pear River Mouth Basin and Qiongdongnan Basin were regarded as the offshore extension of the Cathaysia Block in light of their basin basement (Sun et al., 2014). The Pearl River Mouth Basin, has a basement dominated by Mesozoic granitoids and sedimentary rocks, with Paleozoic metasedimentary rocks scattered in the western part (Sun et al., 2014).

2.2. Regional Tectonics of Palawan

The northeast-southwest oriented islands of Palawan are approximately 450 km long and separate the Sulu Sea from the SCS (Figure 1). In the northwest Sulu Sea basin lies the submerged Cagayan Ridge which is the extinct volcanic arc associated with subduction of the Proto-SCS beneath the Northwest Sulu Sea (Holloway, 1982; Rangin & Silver, 1991).

Palawan is commonly divided into two discrete tectonic terranes, northern Palawan and central-southern Palawan, along the north-south trending Ulugan Bay fault (Schlüter et al., 1996; Yumul et al., 2009) (Figure 2a). Northern Palawan is subdivided into the Malampaya Sound Group in the north and the Barton Group in the south (Figure 2a). The Malampaya Sound Group consists of Permian–Jurassic chert and Jurassic–Early Cretaceous terrigenous clastics, bearing Carboniferous–Jurassic limestone blocks. This group was interpreted as the accretionary prism formed along the South China margin during the Middle Jurassic–Early Cretaceous (Zamoras & Matsuoka, 2004). However, the terrigenous clastic unit, known as the Guinlo Formation, was recently assigned to the Late Cretaceous using the youngest detrital zircon ages (Padrones et al., 2017; Shao, Cao, et al., 2017). The Barton Group is composed of sedimentary and low- to middle- grade metasedimentary rocks and were thought to be deposited along the South China margin (e.g. Suggate et al., 2014; Walia et al., 2012). The depositional age is poorly constrained as Late Cretaceous based on the presence of calcareous nannofossil Prediscosphaera cretacea (Arkhangelsky) (Wolfart et al., 1986) and the youngest detrital zircon ages (Walia et al., 2012). Intrusions of diverse ages, including Late Cretaceous, Middle Eocene and Middle Miocene granites sparsely crop out in northern Palawan (Padroens et al., 2017) (Figure 2a). The St. Paul Limestone north of the Ulugan Bay fault (Figure 2b) represents one of the onshore correlative equivalents of the Nido Limestone. The St. Paul Limestone was ambiguously assigned to the Early Miocene (Wolfart et al., 1986) or the Late Oligocene–Early Miocene (Aurelio & Peña, 2010), based on large benthic foraminifera.

To the southwest of the Ulugan Bay fault, central-southern Palawan is composed of two contrasting units, the Cretaceous–Eocene Palawan Ophiolite and Cenozoic sedimentary sequences (Figure 2a). The Palawan Ophiolite is primarily made up of Eocene oceanic lithosphere of the Northwest Sulu Sea basin emplaced onto the Palawan microcontinental block during Miocene arc microcontinent collision, along with allochthonous remnants of the Cretaceous Proto-SCS oceanic lithosphere (Keenan et al., 2016). The Cenozoic sedimentary sequences were assumed to be an emergent imbricated thrust belt or accretionary prism subsequent to the Miocene collision (Hinz & Schlüter, 1985; Steuer et al., 2013). Some researchers (e. g. Lai et al., 2020) did not regard central-southern Palawan as part of the Palawan microcontinental block and placed central southern Palawan in the southern margin of the Proto-SCS before the elimination of the Proto SCS, in light of the widespread ophiolite in central-southern Palawan. However, the Palawan Ophiolite has not only been obducted onto the Panas-Pandian Formation in central-southern Palawan, but has also been thrust over

the Barton Group and St. Paul Limestone north of the Ulugan Bay fault (e.g. Keenan, 2016) (Figure 2b). Therefore, the Palawan Ophiolite should be treated as an allochthonous block to both northern and central-southern Palawan, and the difference between northern and central-southern Palawan is primarily in the exhumation level of the ophiolite (Ilao et al., 2018). The exhumation level of the ophiolite is much greater in northern Palawan than in central-southern Palawan. Moreover, the turbidites of the Panas-Pandian Formation exposed on central-southern Palawan appear to be the onshore continuation of syn-rift sediments found in half-grabens on the microcontinental block offshore Palawan (Sales et al., 1997; Ding et al., 2015; Aurelio et al., 2014). Therefore, we follow Hall (2002, 2012) inferring that both northern and central-south Palawan belong to the Palawan microcontinent block (Figure 1).

2.3. Cenozoic sedimentary stratigraphy in central-southern Palawan

The Cenozoic sedimentary strata in central-southern Palawan include the Paleogene Panas and Pandian Formations, the Early Miocene Ransang Limestone and the Middle Miocene– Pleistocene collisional-related clastics and carbonates (Isugod Formation, Alfonso XIII Formation and Iwahig Formation) (Aurelio & Peña, 2010; Aurelio et al., 2014) (Figure 2b). The Panas Formation is a turbidite sequence composed mainly of medium- to thin-bedded alterations of sandstone, siltstone and shale (Aurelio & Peña, 2010). A wide age range spanning the Paleocene to Late Eocene was proposed by Wolfart et al. (1986) due to the occurrence of Paleocene–Early Eocene foraminifera and late Middle Eocene–Early Oligocene calcareous nannofossils. The Pandian Formation is dominantly made up of massive coarse-grained sandstone with indurated mudstone and silty shale interbeds downsection (Aurelio & Peña, 2010). Considering the similarities in lithology and estimated age between the Panas Formation and Pandian Formation, Macc and Agadier (1988) suggested that the name Pandian be adopted for the turbidites mapped as Panas Formation, while Aurelio et al. (2014) regarded the Pandian Formation as the s trongly indurated to mildly metamorphosed facies of the Panas Formation. It is difficult to distinguish them in the field. Therefore, for the purposes of this study, we consider them together as the Panas-Pandian Formation. The Panas-Pandian Formation is mainly distributed around the Palawan Ophiolite in southern Palawan, and occurs in a tectonic window near Aborlan in central Palawan (Figure 2b). The poorly exposed Ransang Limestone consists of massive to bedded limestone bearing Early Miocene large foraminifera (Macc & Agadier, 1988) and is correlative to the post-rift Nido Limestone widespread offshore Palawan and the St. Paul Limestone north of the Ulugan Bay fault (Aurelio & Peña, 2010). A Miocene arc-

microcontinent collision led to a complex contact between the Cenozoic sedimentary sequences and the Palawan Ophiolite. The northwestward thrusting of the ophiolite over the Panas-Pandian Formation formed a tectonic window in central Palawan. Along the fringe of the tectonic window, the Panas-Pandian Formation was metamorphosed (Inagauan Metamorphics, Figure 2b). The thrust contact was reversely sealed by Miocene clastics of the Isugod Formation (Aurelio et al., 2014).

3. Methods

Samples of the Panas-Pandian Formation were collected for micropaleontology, trace element, Nd isotope and heavy mineral analyses and detrital zircon U-Pb geochronology to reconstruct the biostratigraphic framework, sedimentary environment, routing and provenance of central-southern Palawan prior to the opening of the SCS. Field investigation was mainly conducted along the coast, road cuts and valleys to obtain the freshest possible samples (Figures 2b and 3). Nineteen mudstone samples were collected for planktonic and benthic foraminiferal and calcareous nannofossil analyses, of which 11 samples were chosen for trace element and Nd isotopic analyses. Four sandstone samples were collected for heavy mineral analysis and two samples were selected for detrital zircon U-Pb dating, to complement the data from sample AB-02f reported by Yan et al. (2018). Planktonic and benthic foraminifera were separated from 200 g of mudstone using conventional methods. Foraminiferal tests from the 100-mesh screen were picked for identification and counting under a stereomicroscope. Standard zonations of planktonic foraminifera established from low-latitude regions by Blow (1969) and datum planes (FAD: first appearance datum; LAD: last appearance datum) as documented by Wade et al. (2011) were followed (Figure 4). Five to 10g of each sample were prepared for calcareous nannofossil analysis employing standard smearslide techniques. More than 100 random fields of view from each slide were examined under a polarizing microscope with 1600x magnification. The zonal scheme of calcareous nannofossils proposed by Martini (1971) and datum planes compiled by Anthonissen and Ogg (2012) were applied (Figure 4).

Mudstones for trace element and Nd isotopic analyses were leached with 2N acetic acid to remove carbonates. Solid residues were collected after centrifuging, oven dried and ground to powder <75 μm. Powders were then heated to 700°C to destroy organic material prior to element and isotopic analyses at the State Key Laboratory of Isotope Geochemistry, Guangzhou Institute of Geochemistry, Chinese Academy of Sciences (GIGCAS). Trace elements were measured on a Perkin-Elmer Sciex Elan 6000 inductively coupled plasma

mass spectrometer (ICP-MS). The analytical procedures followed the method described by Liu et al. (1996). The precision is generally better than 5%. Several USGS and Chinese rock standard references including BHVO-2, GSR-1 and GSD-9 were repeatedly measured with the samples, yielding values generally within ±10% (RSD) of the certified values. Nd measurements were performed on a MicroMass Isoprobe multicollector inductively coupled plasma mass spectrometer (MC-ICP-MS). For details of the methods, see Wei et al. (2002). The measured $^{143}Nd/^{144}Nd$ ratios were normalized to $^{146}Nd/^{144}Nd=0.7219$. A standard Nd solution, Shin Etsu JNdi-1, was repeatedly measured with the samples to monitor the quality of measurements, yielding a mean value of 0.512111±6 (2σ, N=5).

Sandstones for heavy mineral analysis and detrital zircon U-Pb dating were disaggregated and then passed through a 40-mesh sieve. Detrital heavy mineral components were separated by centrifugal elutriation, and further mineral separation was achieved by magnetic and electrostatic filters and heavy liquid. At least 700 non-opaque heavy mineral grains were identified and counted under the binocular microscope for each sample. Around 300 zircon grains were handpicked from the heavy mineral fractions and mounted in epoxy resin for U-Pb isotopic analysis. The location of analytical spots were informed by grain cathodoluminescence images, avoiding inherited cores where possible (Fig S1). Zircon U-Pb dating was performed by laser ablation-inductively coupled plasma-mass spectrometry (LA-ICP-MS) at the Key Laboratory of Mineralogy and Metallogeny, GIGCAS. The instrumentation is composed of an Agilent 7900a ICP-MS coupled with a Resonetic RESOLution S155 ArF-Excimer laser source (k=193 nm). U, Th, and Pb concentrations were calibrated using ^{29}Si as an internal standard and the standard silicate glass NIST 610 as reference material. Zircons 91500 (Reference age 1064 ± 0.8 Ma) (Wiedenbeck et al., 2004) and Plešovice (Reference age 337 ± 0.4 Ma) (Sláma et al., 2008) were used as the standard. Analyses were conducted with a beam diameter of 30 μm; each analysis includes 30 s of gas blank followed by 60 s of data aquisition. Isotope ratios were calculated using ICPMSDataCal 7.7 (Liu et al., 2010).The relative age probability of detrital zircons was processed using Isoplot (Version 3.23) (Ludwig, 2003). Ages with discordance >10% were excluded from the discussion. $^{206}Pb/^{238}U$ and $^{207}Pb/^{206}Pb$ ages were adopted for zircons younger and older than 1000 Ma, respectively.

4. Results

4.1. Field Occurrence

Outcrops of the Panas-Pandian Formation are generally sparse owing to the humid tropical climate and lush vegetation in central-southern Palawan. The observed outcrops are restricted to road cuts, coast and valleys and are dominated by massive sandstones and alternating interbeds of sandstone and mudstone. The massive sandstone mainly occurs along the western coast of southern Palawan (e.g. Sites RZ-01 and RZ-10) and is typically fresh, grey-green, lithic-rich with occasional pebbles of limestone (Figures 2b and 3a). Grading is well developed fining upwards. Sedimentary structures of the massive sandstones are consistent with middle fan deposits of a submarine fan.

Alternations of medium- to thick- bedded sandstone and thin-bedded mudstone are exposed along the road cuts between Quezon and Rizal, slightly east of the coastline (Figure 2b). They are yellowish-brown as a result of strong weathering (Figure 3b). A rare outcrop of relatively unweathered rock consisting of interbeds of light-grey thin-bedded sandstone and thick-bedded mudstone was found at Site RZ-12 (Figure 3c). Trace fossil Helminthopsis are well preserved within sandstone soles (Figure 3d). Helminthopsis is a pascichnion, a structure produced in response to feeding during locomotory activity, of worm-like organisms (Han & Pickerill, 1995). It was commonly reported from deep-water (slope and basinal) flysch sequences, typically as an integral component of Nereites ichnofacies defined by Seilacher (1967). The Panas-Pandian Formation inside the tectonic window in central Palawan (e.g. Site AB-02) is very-weakly metamorphosed, composed of interbeds of highly indurated medium- to thick-bedded sandstone with parallel bedding and thin-bedded shale (Figures 3e and 3f). Based on the above observations, these sandstone-mudstone interbeds were most likely deposited in the middle-lower fan environment.

The attitude of the strata between the observed outcrops is highly variable, and folds are locally developed. In general, the strata dips 10°–70° towards northeast to southeast (Figure 2b). It would be difficult to determine the stratigraphic position of the samples collected from different outcrops because the sparse distribution of the outcrops and the variations of attitude between adjacent outcrops. Nevertheless, in light of the general eastward dip of the strata, we infer that the massive sandstones exposed along the western coast (e.g. Sites RZ-01 and RZ-10) and the alternating sandstone-mudstone sequences along the road cuts between Quezon and Rizal (e.g. Sites RZ-04 and RZ-12) in southern Palawan lie in the lower part of the Panas-Pandian Formation, while the alternating sandstone-mudstone sequences in the tectonic window in central Palawan (Site AB-02) lie in the upper part of the Panas-Pandian Formation.

4.2. Biostratigraphic result

Only three samples at Site RZ-12 of the 19 analyzed samples yielded rare but age-diagnostic planktonic foraminifers and calcareous nannofossils (Figures 5a and 5b). Calcareous microfossils in other outcrops were probably lost to the intense weathering. The identified planktonic foraminifers (7 species belonging to 6 genera) and calcareous nannofossils (14 species belonging to 7 genera) are listed in detail in Tables S1 and S2. The planktonic foraminiferal assemblage is dominated by those spanning the Early Eocene to the Middle Eocene, including *Acarinina cuneicamerata* (Blow) (FAD at 50.20 Ma), *Acarinina bullbrooki* (Bolli) (LAD at 40.49 Ma), *Morozovelloides crassatus* (Cushman) (LAD at 38.25 Ma) and *Globigerinatheka subconglobata* (Shutskaya) (P9–P14; Middle Eocene) with characteristic sub-spherical test (Figure 5a), and thus indicating a wide age range of Zones P9–P12 (50.2–40.5 Ma) (Figure 4). There are also calcareous nannofossil assemblage of *Discoaster lodoensis* Bramlette and Riedel (FAD at 53.70 Ma; LAD at 47.41 Ma), *Discoaster kuepperi* Stradner (NP12–NP14b; Early to Middle Eocene), *Discoaster gemmifer* Stradner (NP12–NP16; Early to Middle Eocene), *Nannotetrina cristata* (Martini) (FAD at 47.73 Ma; LAD at 41.85 Ma), *Sphenolithus spiniger* Bukry (NP14–NP15; Middle Eocene), *Discoaster barbadiensis* Tan (LAD at 34.76 Ma) and *Discoaster saipanensis* Bramlette and Riedel (LAD at 34.44 Ma; NP15–NP20; Middle to Late Eocene) (Figure 5b). Because the FAD of *D. saipanensis* within Zone NP15 has a large uncertainty (Perch-Nielsen, 1985), it is difficult to determine whether *D. lodoensis* and *D. kuepperi* are indigenous or reworked. We thus assign this assemblage to Zones NP14b–NP16 (47.7–41.9 Ma) (Figure 4), which is consistent with the planktonic foraminiferal data. Therefore, the depositional age range of the Panas-Pandian Formation at Site RZ-12 is placed within the Middle Eocene (47.7–41.9 Ma) (Figure 4).

Abundant and diverse benthic foraminifera, characterized by deep-water agglutinated taxa, were recovered from 11 samples (Figure 5c and Table S3). There are frequent occurrences of *Haplophragmoides walteri* (Grzybowski), *Nothia excelsa* (Grzybowski), *Psammosiphonella discreta* (Brady), *Psammosphaera irregularis* Grzybowski and *Trochammina globigeriniformis* (Parker and Jones), with sporadic occurrences of *Ammodiscus tenuissimus* Grzybowski, *Haplophragmoides eggeri* Cushman, *Haplophragmium horridum* Grzybowski, *Haplophragmoides* spp., *Pseudonodosinella elongata* (Grzybowski), *Reticulophragmium amplectens* (Grzybowski), *Saccammina grzybowskii* (Schubert) and *Trochamminoides subcoronatus* (Grzybowski). These agglutinated foraminifera are common in Eocene “flysch-type” deep-water assemblages of the North Atlantic and western Tethys (Kaminski & Gradstein, 2005). The “flysch-type”

fauna indicates middle bathyal to abyssal environments with an upper depth limit of ~500 m (Kaminski & Gradstein, 2005). There are also rare calcareous benthic foraminifera (*Pseudonodosaria* sp., *Lenticulina* sp., *Cibicides* sp. and *Planulina* sp.) in Site RZ-12 samples (Figure 5c).

4.3. Trace element and Nd isotope results

Results of trace element and Nd isotopic analyses of the silicate fraction of the Panas-Pandian Formation mudstones are listed in Tables S4 and Table 1, respectively.
Trace elements that are common in acidic rocks, Rb, Th, U, Nb, Zr, Hf and Y in the Panas-Pandian Formation, except Samples RZ-03b and RZ-06c, show higher concentrations compared to reference Upper Continental Crust (UCC) values (Rudnick & Gao, 2003) (Figure 6a). Abundances of transitional elements, V and Sc in the Panas-Pandian Formation are lower to slightly higher than those of the UCC, while Co, Cr and Ni are significantly lower than those of the UCC (Figure 6a). Such trace element patterns suggests an acidic crustal provenance. Chondrite-normalized distribution patterns of rare earth element (REE) concentration in the Panas-Pandian Formation are similar to those of the UCC, displaying light REEs enrichment, heavy REEs depletion and a negative Eu anomaly (Figure 6b).

The $^{143}Nd/^{144}Nd$ ratios of the Panas-Pandian Formation mudstones are mainly in the range from 0.512162 to 0.512338, corresponding to a εNd range from -9.3 to -8.3 (with an average of -8.7) (Table 1).

4.4 Heavy minerals and detrital zircon U-Pb geochronology

The percentages of non-opaque heavy minerals of four sandstone samples are listed in Table S5 and shown in Figure 7. Samples RZ-10b, RZ-12b and AB-02f have remarkably high percentages of zircon ranging from 73.5%–92.8%, which is consistent with previous results (average value=81.2%) of Shao, Cao, et al. (2017). Whilst Shao, Cao, et al. (2017) only find minor abundances of tourmaline (≤1.1%) and rutile (≤2.7%), our samples RZ-10b and RZ-12b show significantly higher contents of tourmaline (15.6–16.6%) and rutile (4.7%–6.4%). Nevertheless, the high ZTR index (zircon + tourmaline + rutile) in samples RZ-10b, RZ-12b and AB-02f as well as samples of Shao, Cao, et al. (2017) indicate an acidic crustal provenance. Zircon grains are subangular to subrounded in Samples RZ-10b and RZ-12b. In contrast, they are mostly unabraded, angular to subangular in Sample AB-02f (Figure S1), making it unlikely that they have travelled far by fluvial transport. Particularly, Sample RZ-01 has much lower content of zircon (12.1%) and is dominated by unstable mineral of epidote

(64%) and garnet (9.2%) which indicate the existence of metamorphic source. There is also minor but noteworthy Cr-spinel (10.9%) suggesting a local basic-ultrabasic/ophiolitic provenance. The low ZTR index and high abundances of unstable mineral might reflect a short transport distance.

Detrital zircon U-Pb age results are detailed in Table S6. Zircon grains extracted from our samples are light pink, light yellow to colorless, and euhedral to subhedral. Most of the grains show oscillatory zoning typical of magmatic origin (Figure S1). Th/U ratios of the zircons are generally > 0.3 also consistent with an igneous origin. Only a few grains possess Th/U ratios < 0.1 corresponding to a metamorphic origin (Corfu et al., 2003) (Figure S2). Zircon U-Pb ages spans a wide spectrum, from 93 Ma to 3400 Ma (Figures 8a, 8b and 8d). In Sample RZ-01, zircons younger than 200 Ma make up 56% of the total grains analysed and consist of two Mesozoic groups of 90–150 Ma and 160–200 Ma with peaks at ~110 Ma and 177 Ma, respectively (Figure 8a). Two minor age groups are seen at 200–300 Ma and 1700–2100 Ma. The remaining zircons show scattered age distributions from; 400 to 500 Ma, 900 to 1100 Ma and 2200 to 2600 Ma. In Sample RZ-12b, zircons younger than 200 Ma account for 35% of the total zircons (Figure 8b). and these comprise two groups spanning 90–140 Ma and 140–200 Ma, with well developed peaks at ~108 Ma and ~153 Ma, respectively. There are also three age groups of 200–300 Ma, 380–480 Ma and 500–1200 Ma, and a few ages between 1500 to 3400 Ma. We note that the age distribution in this sample is quite similar to that in Sample P027 of Shao, Cao, et al. (2017) (Figure 8c). In contrast, Sample AB-02f (Yan et al. 2018) contains over 87% Mesozoic zircons clustered in 90–200 Ma, with major age peak at 109 Ma and subordinate peak at 151 Ma (Figure 8d).

5. Discussion

5.1. Age of breakup unconformity of the Palawan microcontinental block

In classical models of continental breakup, the transition from rifting of continental crust to onset of seafloor spreading and drifting is often marked by a prominent breakup unconformity on the conjugate continental margins, as the result of breakup induced isostatic uplift that leads to localized erosion (Driscoll et al., 1995; Franke et al., 2013; Morley, 2016). This erosional unconformity typically truncates syn-rift sediments in half-graben basins and separates them from the drape of post-rift sediments (Franke et al., 2013). So far, the age of the breakup unconformity on the northern SCS margin has been extensively investigated, displaying a diachronous southwestward younging trend consistent with seafloor spreading propagating from northeast to southwest (e.g. Franke et al., 2013; Morley, 2016; Zhou et al.,

1995) (Figure 9). In the northeast, Cenozoic strata of the Taixinan Basin exposed on the Western Foothills and the Hsüehshan Range in Taiwan show a regional breakup unconformity between ~39 Ma and ~33 Ma (e.g. Huang et al., 2013, 2017). To the south of the Pearl River Mouth Basin, IODP Expedition 349 penetrated the breakup unconformity at Site U1435 and dated it to ~34 Ma based on the marine microfossils in the post-rift sediments (Li et al., 2017). Within the Pearl River Mouth Basin, the breakup unconformity was placed around the regional marker horizon T7 at ~30 Ma (e.g. Chen et al., 2003; Xie et al., 2014). For the Qiongdongnan Basin in the west, the breakup unconformity was assigned to 23–22 Ma (Zhou et al., 1995).

On the southern SCS margin, the breakup unconformity seen in the Reed Bank area and offshore Palawan is directly capped by a widespread carbonate platform (Nido Limestone) (Franke, 2013). Due to the scarcity of boreholes penetrating syn-rift sediments, the breakup unconformity of the Palawan microcontinental block has only been constrained by the post-rift Nido Limestone.

The onset of the Nido Limestone deposition was controlled by the syn-rift deformation leading to a rugged seafloor relief and varied from the Early Oligocene to the early Early Miocene in wells offshore Palawan (Steuer et al., 2013). Among these wells, the base of the Nido Limestone in well Busuanga-1 offshore northwest Palawan (Figure 1) has been estimated to be as old as the Early Oligocene (~32 Ma) from the top of planktonic foraminiferal Zone N2 (~26 Ma) located above ~200 m above the base of the limestone (Steuer et al., 2013). The limestone deposition in the wells offshore Palawan continued until the early Middle Miocene (~15 Ma) (Steuer et al., 2013). The syn-rift Panas-Pandian Formation cropping out in central-southern Palawan might help to provide more reliable age constraint for the breakup unconformity on the Palawan microcontinental block.

Our integrated biostratigraphic study shows that the Panas-Pandian Formation at Site RZ-12 was deposited in the Middle Eocene (47.7–41.9 Ma). However, Wolfart et al. (1986) reported Paleogene–Early Eocene planktonic foraminifera and late Middle Eocene–Early Oligocene calcareous nannofossils from the Panas Formation. Here we apply the datum planes calibrated by Wade et al. (2011) and Anthonissen & Ogg (2012) to refine the age of these microfossils. The planktonic foraminifera were only recovered from Sample PD 104 in central Palawan (Figure 2b) and comprise *Subbotina velascoensis* (Cushman) (LAD at 55.07 Ma; P3b–P6a), *Globigerina gravelli* (Brönnimann) (synonym of *Acarinina esnehensis* (Nakkady) (P5–P8)), *Acarinina soldadoensi*s (Brönniman) (FAD at 57.79 Ma; P4c-P9), Morozovella aequa (Cushman and Renz) (FAD at 57.79 Ma, LAD at 54.20 Ma; P4c-P6b),

Globanomalina chapmani (Parr) (P3–P5), *Morozovella subbotinae* (Morozova) (FAD at 57.10 Ma, LAD at 50.67 Ma; P5–P7) and *Acarinina wicoxensis* (Cushman and Ponton) (P5 P7), which indicate a narrow age range of Zones P5–P6a (57–55 Ma). However, the appearance of younger species like *Subbotinae linaperta* (Finlay) (LAD at 37.96 Ma; P7–P15) in the same sample is inconsistent with the narrow age range of Zones P5– P6a (57–55 Ma). Moreover, a neighboring sample (PD106) contains younger (43.3–32.9 Ma) calcareous nannofossils (which will be discussed later). Therefore, *S. linaperta* should be recognized as an indigenous fossil, while the Late Paleocene–Early Eocene (57–55 Ma) planktonic foraminiferal assemblage, especially *S. velascoensis, M. aequa and G. chapmani,* are of reworked origin. As a result, we do not adopt the age of Late Paleocene–Early Eocene (57–55 Ma) for the Panas-Pandian Formation. The calcareous nannofossils came from eight samples scattered across central-southern Palawan (six from central Palawan and two from southern Palawan) (Wolfart et al., 1986) and include age-diagnostic species like *Ericsonia formosa* (Kamptner) (LAD at 32.92 Ma), *Reticulofenestra bisecta* (Hay, Mohler and Wade), *Reticulofenestra umbilica* (Levin) (FAD at 43.32 Ma; LAD at 32.02 Ma) and *Sphenolithus predistentus* (Bramlette and Wilcoxon) (LAD at 26.93 Ma). These species suggest an age of Zones NP15c-NP21 (43.3–32.9 Ma) and is younger than the microfossils (47.7–41.9 Ma) recovered from Site RZ-12 (Figure 4). Therefore, these calcareous nannofossils mainly recovered from central Palawan are likely to be taken from the upper part of the Panas-Pandian Formation, while Site RZ-12 at southern Palawan might belong to the lower part of the Panas-Pandian Formation. This is consistent with the inference from field observation that the massive sandstones and the alternating sandstone-mudstone sequences in southern Palawan lie in the lower part of the Panas-Pandian Formation, while the alternating sandstone-mudstone sequences in central Palawan lie in the upper part of the Panas-Pandian Formation. Considering both the present and previous results, we assign the syn-rift Panas Pandian Formation to the Middle Eocene–earliest Oligocene (47.7–32.9 Ma) (Figure 4). It is broadly consistent with the late Early Eocene–Late Eocene age as indicated by the deep-water agglutinated foraminifera (Figure S1) that are widespread in our samples, although agglutinated benthic foraminifera are not as accurate and extensively used as planktonic foraminifera and calcareous nannofossils for the biostratigraphy of Cenozoic marine sediments. A calcareous nannofossil assemblage indicative of 43.3–32.9 Ma was also found in the syn-rift sediments in northwestern Mindoro (Concepcion et al., 2012). At a regional scale this implies that the youngest syn-rift sediments along the Palawan microcontinental block date to around 33 Ma.

The onshore correlative equivalent of the Nido Limestone in central-southern Palawan, known as the Ransang Limestone (Early Miocene), only occurs as small, patchy remnants in central-southern Palawan (Aurelio & Peña, 2010) and was not found during our fieldwork. We suggest that the Ransang Limestone should be treated as part of the Nido Limestone spanning the Early Oligocene (~32 Ma) to the early Middle Miocene (~15 Ma) (Steuer et al., 2013) (Figure 9). Although no contact between the Panas-Pandian Formation and the Ransang Limestone has been observed onland central-southern Palawan, the syn-rift structures and sedimentary fills truncated by a prominent seismic reflector corresponding to the Nido Limestone were observed in seismic profiles offshore Palawan (Steuer et al., 2013; Aurelio et al., 2014). By integrating both the outcrop and subsurface data, the breakup unconformity of the Palawan microcontinental block between the Panas-Pandian Formation and the Nido Limestone can be constrained to 33–32 Ma (Figure 9).

This age reveals that the unconformity is a short hiatus in response to the breakup of the South China margin. The sharp change in sedimentation from siliciclastics to carbonates across the unconformity reflects a lack of terrigenous supply owing to the southward drifting of the Palawan microcontinental block following continental breakup. For the Dangerous Ground area, the breakup unconformity is younger, with a diachronous Late Oligocene age (i.e. around 28–23 Ma, Steuer et al., 2014; Morley, 2016). The breakup unconformity along the southern SCS margin also shows a southwestward younging trend similar to the northern SCS margin. The age of the breakup unconformity of the Palawan microcontinental block (33–32 Ma) is different to that of the Qiongdongnan Basin (23–22 Ma) (Zhou et al., 1995) but is close to that of the Pearl River Mouth Basin (~30 Ma) (Chen et al., 2003; Xie et al., 2014) and IODP Site U1435 (~34 Ma) (Li et al., 2017), suggesting that the Palawan microcontinental block is the counterpart of the Pearl River Mouth Basin in the southern SCS margin. It is noteworthy that the age of the breakup unconformity of the Palawan microcontinental block also overlaps with that of the Taixinan Basin (Taiwan region, 39–33 Ma) (e.g. Huang et al., 2013, 2017). It is difficult to exclude the conjugate relationship between the Palawan microcontinental block and the Taixinan Basin only based on the age of the breakup unconformity. However, the conjugate relationship between the Palawan microcontinental block and the Pearl River Mouth Basin is also evidenced by the flow-line patterns defined from the seafloor spreading lineaments and the fracture zones within the SCS (Sibuet et al., 2016) (Figure 9), which also proved that the Taiwan segment, corresponding to the Taixinan Basin in this study, has no counterpart on the southern SCS margin.

5.2. Paleoenvironment of central-southern Palawan in the Middle Eocene–earliest Oligocene

The Palawan microcontinental block was part of the South China margin and attached to the Pearl River Mouth Basin before opening of the SCS in light of the timing of the breakup unconformity and the flow-line patterns within the SCS (Sibuet et al., 2016). The sedimentary environment of the Panas-Pandian Formation in central-southern Palawan can therefore aid understanding of the paleogeography of the South China margin as well as sediment routing across the continental margin. The Panas-Pandian Formation had a middle-lower fan setting and contained trace fossil Helminthopsis typical of Nereites ichnofacies and 'flysch type' deep-water agglutinated foraminiferal assemblage. The above evidence suggests middle bathyal to abyssal depths (>500 m), such that the Middle Eocene–earliest Oligocene depositional environment was confined to the continental slope and abyssal plain.

In contrast, the syn-rift sediments in the half grabens on the northern SCS margin are mostly deposited in non-marine fluvial to lacustrine environments (Gong & Li, 1997; Yang et al., 2012). Although the marine influence might have expanded southwestward from the East China Sea- Taiwan region to the northern SCS margin, it only occurred in well D21 in the Early to Middle Eocene (shelf to upper-slope environment), in well H15 in the Middle Eocene (shelf to upper-slope environment) and in well B7 in the Late Eocene (shelf environment) (Figure 1) (Li et al., 2017). Microfossils from Eocene syn-rift sediments at IODP Sites U1435, U1501 and U1504 on the distal margin near the continent-ocean boundary also denote coastal and shelf environments (Li et al., 2015; Sun et al., 2018). A deep-water environment (~1000 m depth) was not widespread until the early seafloor spreading stage, as revealed by the Early Oligocene post-rift hemiplegic sediments recovered from Ocean Drilling Program (ODP) Site 1148 and IODP Sites U1435 and U1501 (Li et al., 2015; Wang et al., 2000; Sun et al., 2018). IODP Expedition 368 obtained diverse abyssal agglutinated benthic foraminifera from the Late Eocene syn-rift sediments at Site U1502, but such deep-water conditions are linked to the final stage of continental breakup (the latest Eocene), approaching the initiation of the seafloor spreading (Jian et al., 2019; Larsen et al., 2018). On the southern SCS margin, the Eocene–earliest Oligocene syn-rift sediments in half-grabens on the Reed Bank area and offshore Palawan are dominated by deltaic, littoral and shallow marine deposits, with partly lower neritic to upper bathyal facies in the southeast (Kudrass et al., 1986; Sales et al., 1997; Yao et al., 2012). This

paleoenvironment was intermediate between that of the northern SCS margin and central-southern Palawan, showing a configuration with a southward deepening trend on the South China margin. The southward deepening trend is consistent with an open ocean, named the Proto-SCS by Hinz et al. (1991) that existed on the southern extremities of the South China continental margin at that time. Thus, central-southern Palawan was located on the continental slope of the northern margin of the Proto-SCS (Figure 12).

5.3 Provenance of the Panas-Pandian Formation and its paleogeography implication

5.3.1 Proximal and distal supply from the Cathaysia Block

The trace element and REE distribution patterns of the Panas-Pandian Formation are generally similar to those of the Middle–Late Eocene sediments from IODP Site U1435 and borehole L21 on the northern SCS margin (Shao, Meng, et al., 2017) (Figure 6) and indicate sediment supply from felsic rocks. The high ZTR index in most of the Panas-Pandian Formation sandstones analyzed (except Sample RZ-01) (Figure 7) also denotes derivation from felsic source rocks. In the plots of Cr/V-Y/Ni and Co/Th-La/Sc, the Panas-Pandian Formation samples fall into the field of granite or felsic magmatic rocks, and is of similar range to data from Site U1435 and borehole L21 (Figures 10a and 10b). In the La-Th-Sc and Th-Sc-Zr/10 ternary diagrams, the Panas- Pandian Formation, together with Site U1435 and borehole L21 sediments are plotted between tectonic settings of continental island arc, active continental margin and passive continental margin (Figures 10c and 10d), consistent with the complex tectonic evolution of Cathaysia Block where granitoids are widespread. Therefore, the Panas-Pandian Formation might have a similar provenance to the contemporary Site U1435 and borehole L21 sediments which were mainly derived from the Cathaysia Block (Shao, Meng, et al., 2017; see also Liu et al., 2017). Noteworthy is the abundance of the unstable mineral epidote in Sample RZ-01 (Figure 7) that might imply a local metamorphic source, either the pre-Cambrian metamorphic basement of the Cathaysia Block or the metamorphic rocks related to the Mesozoic subduction along the South China margin, which were uplifted and exhumed by normal faults during the continental rifting (Kudrass et al., 1986). Mesozoic subduction-related ophiolites might account for common Cr-spinel (10.9%) but since epidote and Cr-spinel are rare in all other samples (Figure 7), such local metamorphic and ophiolitic sources would not be common to the Panas-Pandian Formation. No mudstone samples were collected from Site RZ-01 for trace element and Nd isotope analyses because this site is dominated by coarse- to medium-grained sandstone. Therefore,

the ophiolitic source as reflected in the sandstone sample is not observed in the geochemical and isotopic results.

Integrating detrital zircon U-Pb results from this study with previously published work (Shao, Cao, et al., 2017; Yan et al., 2018), the Panas-Pandian Formation is dominated by Cretaceous (90– 140 Ma) and Jurassic (140–200 Ma) zircon grains, with moderate Permian to Triassic (200–300 Ma), Ordovician to Silurian (350–480 Ma) and Mesoproterozoic to Cambrian (500–1200 Ma) zircon grains and minor Paleoproterozoic (1700–2100 Ma) and Archean to Paleoproterozoic (2200–2700 Ma) zircon grains (Figure 8e). This zircon age distribution and the dominant Mesozoic age groups are consistent with a Cathaysian provenance. Similar age distributions are found in modern sediments from the northeastern Pearl River tributaries draining the interior of the Cathaysia Block (Liu et al., 2017; Xu et al., 2007; Zhao et al., 2015) (Figure 8i). We can exclude the Indochina Block and the Yangtze Block as the major source areas for the Panas-Pandian Formation by comparing probability density plots, pie charts (Figure 8) and multidimensional scaling (MDS) plot (Figure 11) of detrital zircon U-Pb age data from the Panas-Pandian Formation with these regions. The modern sediments from the Red River flowing between the Yangtze Block and the Indochina Block (Clift, Carter, et al., 2006; Fyhn et al., 2019; Hoang et al., 2009; Nguyen et al., 2018; Wang et al., 2018), the rivers draining central Vietnam (Truong Son Belt and Kontum Massif of the Indochina Block in Figure 1) (Fyhn et al., 2019; Jonell et al., 2017; Nguyen et al., 2018; Usuki et al.,2013; Wang et al., 2018) and the western Pearl River tributaries primarily draining the Yangtze Block (Liu et al., 2017; Zhao et al., 2015) only contain minor Yanshanian (80–200 Ma) zircon grains generally lower than 7% of the total zircon grains (Figures 8f, 8g and 8h). The abundance of the Yanshanian zircons in the modern sediments from these rivers are significantly lower than the age groups of 200–300 Ma, 300–500 Ma and 500–1500 Ma (Figures 8f, 8g and 8h), contrasting to the dominance of the Yanshanian zircons in the Panas-Pandian Formation samples (Figure 8e). In the MDS plot (Figure 11), the modern sediments from the Red River, the rivers in central Vietnam and the western Pearl River tributaries are grouped together and well separated from the Panas-Pandian Formation samples. Therefore, northern-central Vietnam (the Indochina Block) and the Yangtze Block could not be major sources for the Panas- Pandian Formation. Hainan Island is also unlikely to be major source of central-southern Palawan sediments because Jurassic–Cretaceous granites in Hainan Island are less common than Triassic granites (Shao et al., 2019). By comparing detrital zircon U-Pb age data from the Panas-Pandian Formation with modern sediments from the northeastern Pearl River tributaries and Middle to Late

Eocene sediments from the northern SCS margin (Figure 8 and 11), we infer that the Panas-Pandian Formation was derived from both proximal and distal source regions within the Cathaysia Block.

It is noteworthy that Sample AB-02f in central Palawan shows a unimodal age distribution with an age peak of ~110 Ma which resembles zircon ages from Middle to Late Eocene sediments of IODP Site U1435 (Shao, Meng, et al., 2017) (Figures 8d and 8k). The percentage of the Yanshanian zircon grains of 80–200 Ma is as high as 87% in this sample, even higher than that in Site U1435 sediments (80%). Contemporary sediments from the Pearl River Mouth Basin (Shao et al., 2016, 2019; Wang et al., 2017) generally show a similar restricted age range except for a peak at 44 Ma associated with syn-rift volcanism (Figures 8j). Sediments from two boreholes (ZI- 2 and ZI-3) in the northern Pearl River Mouth Basin have a stronger affinity with the northeastern Pearl River tributaries (Figure 11) probably owing to their proximity to the interior Cathaysia Block. Site U1435 and Pearl River Mouth Basin sediments were interpreted to be primarily eroded from proximal, local basement uplifts that were mainly composed of Mesozoic granitoids (Shao et al., 2016, 2019; Shao, Meng, et al., 2017; Wang et al., 2017). A review of industrial wells in the Pearl River Mouth Basin shows that 94 wells have drilled into the pre-Cenozoic basement (Ye et al., 2018) of which 85 wells intersected granitoids in both structural uplifts and depressions, only 2 wells encountered Mesozoic sedimentary rocks in structural depressions in the easternmost part of the basin. The ages of basement granitoids from 17 wells, determined by zircon U-Pb dating, ranges from 161.6–101.7 Ma (Shi et al., 2011; Xu et al., 2016). Within the Palawan microcontinental block, only the Daroctan Granite is of Late Cretaceous age (87 Ma) in northern Palawan (Padrones et al., 2017), which is younger than the youngest detrital zircon (93.8 Ma) in Sample AB-02f. Therefore, we consider the Mesozoic granitic basement uplifts in the Pearl River Mouth Basin as the most possible source area for Sample AB-02f. Within and around the Pearl River Mouth Basin, detrital zircon U-Pb age data of the Cretaceous sedimentary rock is only available from borehole L23 in the easternmost part of the basin and borehole B23 located near the boundary between the Pearl River Mouth Basin and the Qiongdongnan Basin (Shao, Cao, et al., 2017) and display a unimodal age distribution dominated by Yanshanian zircon grains (Figure 8l). Such a unimodal age distribution is also typical of the Late Cretaceous Barton Group and Guinlo Formation (the terrigenous clastic unit in the Malampaya Sound Group) in northern Palawan (Padrones et al., 2017; Shao, Cao, et al., 2017; Suggate et al., 2014; Walia et al., 2012) (Figure 8m). These Mesozoic sediments/metasediments from the northern SCS margin and Palawan microcontinental block

were interpreted to be derived from the Mesozoic continental arc along the South China margin (e.g. Shao, Cao, et al., 2017). They show close linkage with Sample AB-02f and Site U1435 sediments on the MDS plot (Figure 11). Therefore, Sample AB-02f is also possible to be recycled from the Mesozoic sedimentary rocks in the basement uplifts in the Pearl River Mouth Basin or the Palawan microcontinental block, besides directly eroded from the Mesozoic granitoids.

Samples RZ-12b (Middle Eocene, 47.7–42.1 Ma) and P027 (Shao, Cao, et al., 2017) in southern Palawan share almost the same age distribution pattern as modern sediments from the northeastern Pearl River tributaries (Figures 8a, 8c, 8i and 11). They are characterized by a multimodal age distribution, with a lower percentage of Yanshanian (80–200 Ma) ages (34 36%), and higher percentage of grains with ages between 200–300 Ma (13–14%), 300–500 Ma (18–24%) and 500–1500 Ma (21–27%), relative to the unimodal age distribution. This indicates that samples RZ-12b and P027 were mainly sourced from the interior of the Cathaysia Block where the northeastern Pearl River tributaries drain. Zircon grains of 200 300 Ma and 300–500 Ma might be derived from the Caledonian and Indosinian granitoids restricted along the northern boundary of the Cathaysia Block (Figure 1). Alternatively, these zircon grains, together with the older age groups, could be also recycled from the Paleozoic and Mesozoic sedimentary rocks which are part of the basement of the Pearl River Mouth Basin (Sun et al., 2014) and the Palawan microcontinental block (Franke et al., 2011; Kudrass et al., 1986). However, they seem unlikely to be the major source of Samples RZ-12b and P027. For the Pearl River Mouth Basin, the intrabasinal uplifts are dominated by Mesozoic granitoids in light of the drilling data (Ye et al., 2018). The Palawan microcontinent block was mostly submerged during the Eocene and transient uplift and erosion of the Reed Bank was assumed to occur at the end of the Middle Eocene (Yao et al., 2012) which contradicts with the depositional age of Sample RZ-12b within the Middle Eocene. More importantly, the Cretaceous sediments from the Pearl River Mouth Basin and the Palawan microcontinental block, displaying unimodal age distribution dominated by Yanshanian zircon grains (Figures 8l and 8m), could not supply abundant zircons older than 200 Ma to samples RZ-12b and P027. The Eocene sediments from the Taixinan Basin also exhibit a multimodal age distribution, but generally with much less zircons younger than 500 Ma and much more zircons older than 500 Ma (Figure 8n). Sediments from boreholes ZI-2 and ZI-3 in the northern Pearl River Mouth Basin and from borehole D2 in the Taixinan Basin, showing affinity with the northeastern Pearl River tributaries (Figure 11), might not require a direct sedimentary connection to central southern Palawan. These sediments were likely to be

delivered by other small rivers draining the interior Cathaysia Block given the location of the boreholes.

Therefore, the Panas-Pandian Formation might have two major source regions, a proximal source from the Mesozoic basement uplifts composed of granitic and possibly sedimentary rocks and a distal source from the interior Cathaysia Block. This could be also supported by the age peaks of the Mesozoic zircons. Samples RZ-12b and P027 with a predominantly distal source have a stronger Early Yanshanian peak at ~150 Ma, whereas Sample AB-02f with a predominantly proximal source show a stronger Late Yanshanian peak at ~110 Ma (Figure 8), which is in agreement with the oceanward younging trend of the Yanshanian granitoids as a result of steepening of the subduction angle of the Pacific Plate beneath Eurasia (Li & Li, 2007). The remaining samples in central-southern Palawan might result from mixing of these two sources (Figure 11).

The Nd isotope results of the Panas-Pandian Formation are less effective in discriminating the source areas, because the εNd values of the Panas-Pandian Formation (-9.3 to -8.3) fall into all the ranges of the Cathaysia Block (-15.7 to 11.8), the Yangtze Block (-31.1 to 2.6) and the Indochina Block (-21.8 to 14.8) (Clift, Blusztajn, et al., 2006 and references therein). Nevertheless, they are most close to the major peak of the Cathaysia Block (Figure 10e). It is intriguing that the Panas-Pandian Formation only show small Nd isotopic variation between the analyzed samples (Table 1 and Figure 10e), although two major sources are indicated by the detrital zircon U Pb age data. This could be explained by mixing of two sources with εNd values similar to the Panas- Pandian Formation (-9.3–-8.3). The modern sediments collected from the outlets of the Bei River and the Dong River, which might represent the average composition of the interior Cathaysia Block, show εNd values of -11.2±0.2 and -9.9±0.7, respectively (Liu et al., 2017) (Figure 10e). These εNd values, especially that of the Dong River, are close to the εNd values of the Panas-Pandian Formation. Although no Nd isotope data of the Mesozoic granitoids has been reported from the Pearl River Mouth Basin and the Palawan microcontinental block yet, the Mesozoic Hong Kong granites, which crop out in a small area along the South China coast, might be treated as an alternative to the Mesozoic granitoids exposed in local basement uplifts. The Hong Kong granites, predominately of Jurassic–Cretaceous age, show a wide range of εNd values from -15.7 to 4.4 and (Darbyshire and Sewell, 1997) (Figure 10e). The granite samples (n=40) yield an average value of -7.9, also close to the εNd values of the Panas-Pandian Formation. However, such similarity in εNd values may have resulted from sampling bias of the granite samples. Future Nd isotope work of the Mesozoic granitoids and the granitoid-

derived sediments from the northern SCS margin and the Palawan microcontinental block needs to be done to interpret the small Nd isotopic variation of the Panas-Pandian Formation.

5.3.2. Paleogeographic and tectonic implication for the rifted South China margin

Although a near-modern drainage configuration of the Pearl River had not formed until the Early Miocene (Cao et al., 2018; Liu et al., 2017), a paleo-Pearl River confined to the Cathaysia Block like its modern northeastern tributaries was previously proposed to be established since the late Early Oligocene (Cao et al., 2018; Shao et al., 2016). This scenario is suggested by a large set of southward-prograding deltaic sequence observed in seismic profile across the southern Pearl River Mouth Basin (Pang et al., 2009) and by the multimodal age spectra of detrital zircons in the Lower Oligocene samples of borehole X28 and P33 in the Pearl River Mouth Basin (Shao et al., 2016; Wang et al., 2019). However, in light of the similarity in detrital zircon U-Pb age spectra between Samples RZ-12b and P027 from the Panas-Pandian Formation and modern sediments from the northeastern Pearl River tributaries, the paleo-Pearl River can be dated back to the Middle Eocene (47.7–42.1 Ma) based on the depositional age of Sample RZ-12b. It flowed across the rifted South China margin, delivering sediments from the interior Cathaysia Block to central southern Palawan on the continental slope (Figure 12). This scenario is consistent with a complex Eocene southward-prograding deltaic system observed in the Reed Bank area (Yao et al., 2012). It could be deduced that although the structural uplifts on the rifted South China margin, which act as local sediment source, might obstruct the sediments transported from the interior Cathaysia Block, the structural depressions might serve as passages for these sediments delivered to centralsouthern Palawan during the Middle Eocene–earliest Oligocene. The sediment routing also argues against the existence of a narrow, elongate deep-sea basin/gulf between the northern SCS margin and the area that became the Palawan microcontinental block, otherwise the sediments with affinity of northeastern Pearl River tributaries would not reach central-southern Palawan.

From the evidence presented above we consider that the Panas-Pandian Formation was deposited prior to SCS seafloor spreading when the South China continental margin developed into a wide rift system with a low topographic gradient (Figure 12). Such a wide rift system typically develops on hot, weak continental crust, which is in agreement with the weak crustal rheology of the South China margin relating to its pre-rift history where plate convergence led to crustal thickening and magmatic additions in a continental arc regime shortly before the onset of rifting (Brune et al., 2017; Clift et al., 2002). A deep-water basin

between the Pearl River Mouth Basin and the Palawan microcontinental block did not fully exist until the Latest Eocene, as indicated by deep-water environment sediments at IODP Site U1502 (Jian et al., 2019). This change is consistent with a phase of rapid rifting in the Late Eocene–Early Oligocene, just before final breakup and seafloor spreading (Brune et al., 2016; Larsen et al., 2018). The rift acceleration might result from the successively weakening of the rift center due to necking and strain softening with continued deformation (Brune et al., 2016).

6. Conclusion

Our stratigraphic and provenance work on the syn-rift Panas-Pandian Formation from the southern margin of the Palawan microcontinental block improves understanding of the paleogeography of the South China margin prior to opening of the SCS. Biostratigraphic constraints from planktonic foraminifera and calcareous nannofossils show that the Panas-Pandian Formation was deposited in the Middle Eocene–earliest Oligocene (47.7–32.9 Ma). Therefore, the breakup unconformity on the Palawan microcontinental block, between the syn-rift Panas-Pandian Formation and the post-rift Nido Limestone (as old as ~32 Ma, Steuer et al., 2013) is constrained to 33–32 Ma. This age is close to the age of the breakup unconformity of the Pearl River Mouth Basin (~30 Ma) and IODP Site U1435 (~34 Ma), suggesting that the Pearl River Mouth Basin is the conjugate margin of the Palawan microcontinental block which is also supported by the flowline patterns within the SCS (Sibuet et al., 2016). Trace fossil Helminthopsis and deep-water agglutinated benthic foraminifera observed in the Panas-Pandian Formation indicate middle bathyal to abyssal environment (>500 m water depth), which locates central-southern Palawan on the continental slope of the South China margin in the Middle Eocene–earliest Oligocene. All the results of trace elements, Nd isotope, heavy mineral assemblage and detrital zircon U-Pb geochronology indicate the Cathaysia Block as the potential source area of the Panas-Pandian Formation. The detrital zircon U-Pb age distribution of the Panas-Pandian Formation further suggest two major source regions, a proximal source from local Mesozoic basement uplift (granitic and possibly sedimentary rocks) and a distant source from the interior Cathaysia Block. The distant source indicates the establishment of a paleo-Pearl River like its modern northeastern tributaries at least since the Middle Eocene (47.7–42.1 Ma). It could deliver sediments across the South China margin from the interior Cathaysia Block to central southern Palawan on the continental slope. This source-to-sink transport process implies a

wide rifted margin with a low topographic gradient generated on the hot, weak continental crust of South China before the seafloor spreading.

References

Anthonissen, D. E., & Ogg J. G. (2012). Appendix 3—Cenozoic and Cretaceous biochronology of planktonic foraminifera and calcareous nannofossil. In F. M. Gradstein et al. (Eds.), *The Geologic Time Scale 2012* (pp. 1083–1127). Boston: Elsevier.

Aurelio, M. A., Forbes, M. T., Taguibao, K. J. L., Savella, R. B., Bacud, J. A., Franke, D., Pubellier M., Savva D., Meresse F., Steuer, S., & Carranza, C. D. (2014). Middle to Late Cenozoic tectonic events in south and central Palawan (Philippines) and their implications to the evolution of the south-eastern margin of South China Sea: Evidence from onshore structural and offshore seismic data. *Marine and Petroleum Geology*, *58*, 658–673. https://doi.org/10.1016/j.marpetgeo.2013.12.002

Aurelio, M.A., & Peña, R.E. (Eds.). (2010). *Geology of the Philippines tectonics and stratigraphy*, (Second ed., Vol. 1.). Quezon City, Philippines: Mines and Geosciences Bureau, Department of Environment and Natural Resources.

Barckhausen, U., Engels, M., Franke, D., Ladage, S., & Pubellier, M. (2014). Evolution of the South China Sea: revised ages for breakup and seafloor spreading. *Marine and Petroleum Geology*, *58*, 599–611. https://doi.org/10.1016/j.marpetgeo.2014.02.022

Blow, W. H. (1969), Late Middle Eocene to Recent planktonic foraminiferal biostratigraphy. In P. Brönnimann & H. H. Renz (Eds.), *Proceedings of the First International Conference on Planktonic Microfossils* (vol. 1, pp. 199–422). Leiden: E.J. Brill.

Borissova, I., Coffin, M. F., Charvis, P., & Operto, S. (2003). Structure and development of a microcontinent: Elan Bank in the southern Indian Ocean. *Geochemistry, Geophysics, Geosystems*, *4*(9). https://doi.org/10.1029/2003GC000535

Briais, A., Patriat, P., & Tapponnier, P. (1993). Updated interpretation of magnetic anomalies and seafloor spreading stages in the South China Sea: Implications for the Tertiary tectonics of Southeast Asia. *Journal of Geophysical Research: Solid Earth*, *98*(B4), 6299–6328. https://doi.org/10.1029/92JB02280

Brune, S., Heine, C., Clift, P. D., & Pérez-Gussinyé, M. (2017). Rifted margin architecture and crustal rheology: reviewing Iberia-Newfoundland, central South Atlantic, and South China Sea. *Marine and Petroleum Geology*, *79*, 257–281. https://doi.org/10.1016/j.marpetgeo.2016.10.018

Cao, L., Shao, L., Qiao, P., Zhao, Z., & van Hinsbergen, D. J. (2018). Early Miocene birth of modern Pearl River recorded low-relief, high-elevation surface formation of SE Tibetan Plateau. *Earth and Planetary Science Letters*, *496*, 120–131. https://doi.org/10.1016/j.epsl.2018.05.039

Carter, A., Curtis, M., & Schwanethal, J. (2014). Cenozoic tectonic history of the South Georgia microcontinent and potential as a barrier to Pacific-Atlantic through flow. *Geology*, *42*(4), 299–302. https://doi.org/10.1130/G35091.1

Carter, A., Roques, D., Bristow, C., & Kinny, P. (2001). Understanding Mesozoic accretion in Southeast Asia: Significance of Triassic thermotectonism (Indosinian orogeny) in Vietnam. Geology, *29*(3), 211–214. https://doi.org/10.1130/0091-7613(2001)029<0211:UMAISA>2.0.CO;2

Clift, P. D., Blusztajn J., & Nguyen D. A. (2006). Large-scale drainage capture and surface uplift in Tibet-SW China before 24 Ma inferred from sediments of the Hanoi Basin, Vietnam. *Geophysical Research Letters*, *33*, L19403. https://doi.org/10.1029/2006GL027772

Clift, P., Lin, J., & Barckhausen, U. (2002). Evidence of low flexural rigidity and low viscosity lower continental crust during continental break-up in the South China Sea. *Marine and Petroleum Geology*, *19*(8), 951–970. https://doi.org/10.1016/S0264-8172(02)00108-3

Chen, C., Shi, H., Xu, S., Chen, X. et al. (2003). *Formation Conditions of Tertiary Oil/Gas Reservoirs in Pearl River Mouth Basin (East)*. Beijing: Science Press.

Chen, J. F., & Jahn, B. M. (1998). Crustal evolution of southeastern China: Nd and Sr isotopic evidence. *Tectonophysics*, *284*(1–2), 101–133. https://doi.org/10.1016/S0040-1951(97)00186-8

Concepcion, R. A. B., Dimalanta, C. B., Yumul Jr, G. P., Faustino-Eslava, D. V., Queaño, K. L., Tamayo Jr, R. A. & Imai, A. (2012). Petrography, geochemistry, and tectonics of a rifted fragment of Mainland Asia: evidence from the Lasala Formation, Mindoro Island, Philippines. *International Journal of Earth Sciences*, *101*(1), 273–290. https://doi.org/10.1007/s00531-011-0643-5

Corfu, F., Hanchar, J. M., Hoskin, P. W., & Kinny, P. (2003). Atlas of zircon textures. *Reviews in Mineralogy and Geochemistry*. *53*, 469–500. https://doi.org/10.2113/0530469

Ding, W., Li, J., Dong, C., & Fang, Y. (2015). Oligocene–Miocene carbonates in the Reed Bank area, South China Sea, and their tectono-sedimentary evolution. *Marine Geophysical Research*, *36*(2–3), 149–165. https://doi.org/10.1007/s11001-014-9237-5

Driscoll, N. W., Hogg, J. R., Christie-Blick, N., & Karner, G. D. (1995). Extensional tectonics in the Jeanne d'Arc Basin, offshore Newfoundland: implications for the timing of break-up between Grand Banks and Iberia. *Geological Society, London, Special Publications*, *90*(1), 1–28. https:// doi.org/10.1144/GSL.SP.1995.090.01.01

Franke, D. (2013). Rifting, lithosphere breakup and volcanism: comparison of magma-poor and volcanic rifted margins. *Marine and Petroleum Geology*, *43*, 63–87. https://doi.org/10.1016/j.marpetgeo.2012.11.003

Franke, D., Barckhausen, U., Baristeas, N., Engels, M., Ladage, S., Lutz, R., Montano, J., Pellejera, N., Ramos, E. G. & Schnabel, M. (2011). The continent–ocean transition at the southeastern margin of the South China Sea. *Marine and Petroleum Geology*, *28*(6), 1187–1204. https://doi.org/10.1016/j.marpetgeo.2011.01.004

Franke, D., Savva, D., Pubellier, M., Steuer, S., Mouly, B., Auxietre, J. L., Meresse, F., & Chamot-Rooke, N. (2014). The final rifting evolution in the South China Sea. *Marine and Petroleum Geology*, *58*, 704–720. https://doi.org/10.1016/j.marpetgeo.2013.11.020

Gong, Z., & Li, S. (1997). *Continental Margin Basin Analysis and Hydrocarbon Accumulation of the Northern South China Sea* (in Chinese). Beijing: Science Press.

Hall, R. (2002). Cenozoic geological and plate tectonic evolution of SE Asia and the SW Pacific: computer-based reconstructions, model and animations. *Journal of Asian Earth Sciences*, *20*(4), 353–431. https://doi.org/10.1016/S1367-9120(01)00069-4

Han, Y., & Pickerill, R. K. (1995). Taxonomic review of the ichnogenus *Helminthopsis* Heer 1877 with a statistical analysis of selected ichnospecies. *Ichnos: An International Journal of Plant & Animal*, *4*(2), 83–118. https://doi.org/10.1080/10420949509380118

Hinz, K. & Schlüter, H. U. (1985). Geology of the dangerous grounds, South China Sea, and the continental margin of southwest Palawan: results of Sonne cruises SO-23 and SO-27. *Energy*, *10*(3–4), 297–315. https://doi.org/10.1016/0360-5442(85)90048-9

Hinz, K., Block, M., Kudrass, H. R. & Meyer, H. (1991). Structural elements of the Sulu Sea, Phillipines. *Geologisches Jahrbuch, Reihe A*, *127*, 483–506.

Holloway, N. H. (1982). North Palawan block, Philippines–its relation to Asian mainland and role in evolution of South China Sea. AAPG Bulletin, *66*, 1355–1383. https://doi.org/10.1306/03B5A7A5-16D1-11D7-8645000102C1865D

Huang, C. Y., Yen, Y., Liew, P. M., He, D. J., Chi, W. R., Wu, M. S., & Zhao, M. (2013). Significance of indigenous Eocene larger foraminifera *Discocyclina dispansa* in Western Foothills, Central Taiwan: a Paleogene marine rift basin in Chinese continental margin. *Journal of Asian Earth Sciences*, 62, 425–437. https://doi.org/10.1016/j.jseaes.2012.10.026

Huang, C. Y., Shea, K. H., & Li, Q. (2017). A foraminiferal study on Middle Eocene-Oligocene break-up unconformity in northern Taiwan and its correlation with IODP Site U1435 to constrain the onset event of South China Sea opening. *Journal of Asian Earth Sciences*, *138*, 439–465. https://doi.org/10.1016/j.jseaes.2016.09.014

Huang, C. Y., Shao, L., Wang, M. H., Xue, W. G., Qiao, P. J., Cui, Y. C. & Hou, Y. L. (2019). Benthic foraminiferal fauna and sediment provenance of eocene syn-rift sequences in taiwan: implication for onset of asian epi-continental marginal seas off china coast. *Marine Geophysical Research*, *40*, 111–127. https://doi.org/10.1007/s11001-018-9366-3

Hutchinson, D. R., & Klitgord, K. D. (1988). Evolution of rift basins on the continental margin off southern New England. In W. Manspeizer (Eds.), *Triassic-Jurassic Rifting: Continental Breakup and the Origin of the Atlantic Ocean and Passive Margins*, *Developments in Geotectonics* (Vol. 22, pp. 81–98). New York: Elsevier. https://doi.org/10.1016/B978-0-444-42903-2.50009-9

Jian, Z., Jin, H., Kaminski, M. A., Ferreira, F., Li, B., & Yu, P. S. (2019). Discovery of the marine Eocene in the northern South China Sea. *National Science Review*, *6*(5), 881–885. https://doi.org/10.1093/nsr/nwz084

Kaminski, M. A., & Gradstein, F. M. (2005). *Atlas of Paleogene cosmopolitan deep-water agglutinated foraminifera* (Vol. 10, pp. 1–547). Grzybowski Foundation.

Keenan, T. E., Encarnación, J., Buchwaldt, R., Fernandez, D., Mattinson, J., Rasoazanamparany, C., & Luetkemeyer, P. B. (2016). Rapid conversion of an oceanic spreading center to a subduction zone inferred from high-precision geochronology. *Proceedings of the National Academy of Sciences*, *113*(47), E7359–E7366. https://doi.org/10.1073/pnas.1609999113

Kudrass, H. R., Wiedicke, M., Cepek, P., Kreuzer, H., & Müller, P. (1986). Mesozoic and Cainozoic rocks dredged from the South China Sea (Reed Bank area) and Sulu Sea and their significance for plate-tectonic reconstructions. *Marine and Petroleum Geology*, *3*(1), 19–30. https://doi.org/10.1016/0264-8172(86)90053-X

Larsen, H. C., Mohn, G., Nirrengarten, M., Sun, Z., Stock, J., Jian, Z., et al. (2018). Rapid transition from continental breakup to igneous oceanic crust in the South China Sea. *Nature Geoscience*, *11*(10), 782–789. https://doi.org/10.1038/s41561-018-0198-1

Li, C. F., Xu, X., Lin, J., Sun, Z., Zhu, J., Yao, Y., et al. (2014). Ages and magnetic structures of the South China Sea constrained by deep tow magnetic surveys and IODP Expedition 349. *Geochemistry, Geophysics, Geosystems*, *15*, 4958–4983, https://doi.org/10.1002/2014GC005567

Li, C. F., Lin, J., Kulhanek, D. K., & the Expedition 349 Scientists (2015). South China Sea Tectonics. *Proceedings of the International Ocean Discovery Program*. (Vol. 349). College Station, TX: International Ocean Discovery Program. http://dx.doi.org/10.14379/iodp.proc.349.2015

Li, F., Sun, Z., & Yang, H. (2018). Possible spatial distribution of the Mesozoic volcanic arc in the present-day South China Sea continental margin and its tectonic implications. *Journal of Geophysical Research: Solid Earth*, *123*, 6215–6235. https://doi.org/10.1029/2017JB014861

Li, Q. Y., Wu, G. X., Zhang, L. L., Shu, Y., & Shao, L. (2017). Paleogene marine deposition records of rifting and breakup of the South China Sea: An overview. *Science China Earth Sciences*, *60*, 2128–2140, https://doi.org/ 10.1007/s11430-016-0163-x

Li, Z. X., & Li, X. H. (2007). Formation of the 1300 km-wide intracontinental orogen and post-orogenic magmatic province in Mesozoic South China: A flat-slab subduction model. *Geology*, *35*(2), 179–182. https://doi.org/10.1130/G23193A.1

Li, Z. X., Li, X. H., Chung, S. L., Lo, C. H., Xu, X., & Li, W. X. (2012). Magmatic switch-on and switch-off along the South China continental margin since the Permian: Transition from an Andean-type to a Western Pacific-type plate boundary. *Tectonophysics*, *532*, 271–290. https://doi.org/10.1016/j.tecto.2012.02.011

Liu, C., Clift, P. D., Carter, A., Böning, P., Hu, Z., Sun, Z., & Pahnke, K. (2017). Controls on modern erosion and the development of the Pearl River drainage in the late Paleogene. *Marine Geology*, *394*, 52–68. http://dx.doi.org/10.1016/j.margeo.2017.07.011

Liu, W. N., Li, C. F., Li, J., Fairhead, D., & Zhou, Z. (2014). Deep structures of the Palawan and Sulu Sea and their implications for opening of the South China Sea. *Marine and Petroleum Geology*, *58*, 721–735. https://doi.org/10.1016/j.marpetgeo.2014.06.005

Liu, Y., Liu, H. C., & Li, X. H. (1996). Simultaneous and precise determination of 40 trace elements in rock samples using ICP-MS (in Chinese with English abstract). *Geochimica*, 25 (6), 552–558.

Liu, Y., Hu, Z., Zong, K., Gao, C., Gao, S., Xu, J., & Chen, H. (2010). Reappraisement and refinement of zircon U-Pb isotope and trace element analyses by LA-ICP-MS. *Chinese Science Bulletin*, *55*, 1535–1546. https://doi.org/10.1007/s11434-010-3052-4

Ludwig, K. R. (2003). User's manual for isoplot 3.00, a geochronlogical toolkit for Microsoft Excel. *Berkeley Geochronology Central Special Publication*, 4, 25–32.

Macc, Y. O., & Agadier M. A. (1988). Stratigraphic, paleontologic and sedimentologic studies of southern Palawan: its tectonic implications. *Research on stratigraphic correlation of Cenozoic strata in oil and gas fileds Philippines* (ITIT Project No. 8319, pp. 102–133).

Martini, E. (1971). Standard Tertiary and Quaternary calcareous nanoplankton zonation. In A. Farinacci (Eds.), *Proceedings of the 2nd International Conference on Planktonic Microfossils* (Vol. 2., pp. 739–785). Roma: Tecnosci.

Morley C. K. (2016). Major unconformities/termination of extension events and associated surfaces in the South China Seas: review and implications for tectonic development. *Journal of Asian Earth Sciences*, *120*, 62–86. https://doi.org/10.1016/j.jseaes.2016.01.013

Murray, J. W. (1991). Ecology and palaeoecology of benthic foraminifera. Harlow, Essex, UK: Longman Scientific and Technical.

Pang, X., C. Chen, M. Zhu, M. He, J. Shen, S. Lian, X. Wu, & L. Shao (2009). Baiyun movement: A significant tectonic event on Oligocene/Miocene boundary in the northern South China Sea and its regional implications. *Journal of Earth Science*, *20*(1), 49–56, https://doi.org/10.1007/s12583-009-0005-4.

Padrones J. T., Tani K., Tsutsumi Y., Imai A. (2017). Imprints of Late Mesozoic tectono-magmatic events on Palawan Continental Block in northern Palawan, Philippines. *Journal of Asian Earth Sciences*, 142, 56–76. http://dx.doi.org/10.1016/j.jseaes.2017.01.027

Perch-Nielsen, K. (1985). Cenozoic calcareous nannofossils. In H. M., Bolli, J. B. Saunders, K. Perch-Nielsen (Eds.) *Plankton Stratigraphy: Volume 1, Planktic Foraminifera, Calcareous Nannofossils and Calpionellids* (Vol. 1). CUP Archive.

Rangin, C., & Silver, E. A. (1991). Neogene tectonic evolution of the Celebes-Sulu basins: new insights from Leg 124 drilling. In *Proceedings of the Ocean Drilling Program, Scientific Results* (Vol. 124, pp. 51-63). Ocean Drilling Program. https://doi.org/10.2973/odp.proc.sr.124.122.1991

Rudnick, R. L., & Gao, S. (2003). Composition of the continental crust. In R. L. Rudnick, (Eds.), Treatise on Geochemistry, vol. 3, The Crust (Vol. 3, pp. 1–64). New York: Elsevier.

Sales, A. O., Jacobsen, E. C., Morado Jr., A. A., Benavidez, J. J., Navarro, F. A., & Lim, A. E. (1997). The petroleum potential of deepwater northwest Palawan block GSEC 66. *Journal of Asian Earth Sciences*, *15* (2–3), 217–240. https://doi.org/10.1016/S0743-9547(97)00009-3

Schlüeter, H. U., Hinz, K., & Block, M. (1996). Tectono-stratigraphic terranes and detachment faulting of the South China Sea. *Marine Geology*, *130*, 39–78. https://doi.org/10.1016/0025-3227(95)00137-9

Seilacher, A. (1967). Bathymetry of trace fossils. *Marine Geology*, 5, 413–428. https://doi.org/10.1016/0025-3227(67)90051-5

Shao, L., Cao, L., Pang, X., Jiang, T., Qiao, P., & Zhao, M. (2016). Detrital zircon provenance of the Paleogene syn-rift sediments in the northern South China Sea. *Geochemistry, Geophysics, Geosystems*, *17*(2), 255–269. https://doi.org/10.1002/2015GC006113

Shao, L., Cao, L., Qiao, P., Zhang, X., Li, Q., & van Hinsbergen, D. J. (2017). Cretaceous–Eocene provenance connections between the Palawan Continental Terrane and the northern South China Sea margin. *Earth and Planetary Science Letters*, *477*, 97–107. https://doi.org/10.1016/j.epsl.2017.08.019

Shao, L., Meng, A., Li, Q., Qiao, P., Cui, Y., Cao, L., & Chen, S. (2017). Detrital zircon ages and elemental characteristics of the Eocene sequence in IODP Hole U1435A: implications for rifting and environmental changes before the opening of the South China Sea. *Marine Geology*, *394*, 39–51. https://doi.org/10.1016/j.margeo.2017.08.002

Shao, L., Cui, Y., Stattegger, K., Zhu, W., Qiao, P., & Zhao, Z. (2019). Drainage control of Eocene to Miocene sedimentary records in the southeastern margin of Eurasian Plate. *Bulletin*, *131*(3–4), 461–478. https://doi.org/10.1130/B32053.1

Shi, H. S., Xu, C. H., Zhou, Z. Y., Ma, C. Q. (2011). Zircon U-Pb dating on granitoids from the northern South China Sea and its geotectonic relevance. *Acta Geologica Sinica* (English edition), *85*(6), 1359–1372.

Sláma, J., Košler, J., Condon, D. J., Crowley, J. L., Gerdes, A., Hanchar, J. M., Horstwood, M. S. A., Morris, G. A., Nasdala, L., Norberg, N., Schaltegger, U., Schoene, B., Tubrett, M. N., & Whitehouse, M. J. (2008). Plešovice zircon—a new natural reference material

for U-Pb and Hf isotopic microanalysis. *Chemical Geology*, *249*, 1–35. https://doi.org/10.1016/j.chemgeo.2007.11.005

Steuer, S., Franke, D., Meresse, F., Savva, D., Pubellier, M., Auxietre, J. L., & Aurelio, M. (2013). Time constraints on the evolution of southern Palawan Island, Philippines from onshore and offshore correlation of Miocene limestones. *Journal of Asian Earth Sciences*, *76*, 412–427. https://doi.org/10.1016/j.jseaes.2013.01.007

Steuer, S., Franke, D., Meresse, F., Savva, D., Pubellier, M., & Auxietre, J. L. (2014). Oligocene–Miocene carbonates and their role for constraining the rifting and collision history of the Dangerous Grounds, South China Sea. *Marine and Petroleum Geology*, *58B*, 644–657. https://doi.org/10.1016/j.marpetgeo.2013.12.010

Suggate, S. M., Cottam, M. A., Hall, R., Sevastjanova, I., Forster, M. A., White, L. T., Armstrong, R. A., Carter, M. A., & Mojares, E. (2014). South China continental margin signature for sandstones and granites from Palawan, Philippines. *Gondwana Research*, *26*(2), 699–718. https://doi.org/10.1016/j.gr.2013.07.006

Sun, S. S., McDonough, W. S. (1989). Chemical and isotopic systematics of oceanic basalts: Implications for mantle composition and processes. *Geological Society, London, Special Publications*, *42*(1), 313–345. https://doi.org/10.1144/GSL.SP.1989.042.01.19

Sun, X. M., Zhang, X. Q., Zhang, G. C., Lu, B. L., Yue, J. P., Zhang, B. (2014). Texture and tectonic attribute of Cenozoic basin basement in the northern South China Sea. *Science China: Earth Sciences*, *57*, 1199–1211. doi: 10.1007/s11430-014-4835-2

Sun, Z., Jian, Z., Stock, J. M., Larsen, H. C., Klaus, A., Alvarez Zarikian, C. A., & the Expedition 367/368 Scientists (2018). South China Sea Rifted Margin. *Proceedings of the International Ocean Discovery Program*. (Vol. 367/368). College Station, TX: International Ocean Discovery Program. https://doi.org/10.14379/iodp.proc.367368.2018

Taylor, B., & Hayes, D. E. (1983). Origin and history of the South China Sea basin. In D. E. Hayes, (Eds.), *The Tectonic and Geologic Evolution of Southeast Asian Seas and Islands: Part 2, Geophysical Monograph Series* (Vol. 27, pp. 23–56). Washington, DC: American Geophysical Union. https://doi.org/10.1029/GM027p0023

Theunissen, T., & Huismans, R. S. (2019). Long-term coupling and feedback between tectonics and surface processes during non-volcanic rifted margin formation. *Journal of Geophysical Research: Solid Earth*, *124*(11), 12323-12347. https://doi.org/10.1029/2018JB017235

Vermeesch, P. (2013). Multi-sample comparison of detrital age distributions. *Chemical Geology*, *341*, 140–146. https://doi.org/10.1016/j.chemgeo.2013.01.010

Wade, B. S., Pearson, P. N., Berggren, W. A., & Pälike, H. (2011). Review and revision of Cenozoic tropical planktonic foraminiferal biostratigraphy and calibration to the geomagnetic polarity and astronomical time scale. *Earth-Science Reviews*, *104*(1–3), 111–142. https://doi.org/10.1016/j.earscirev.2010.09.003

Walia, M., Knittel, U., Suzuki, S., Chung, S. L., Pena, R. E. & Yang, T. F., 2012. No Paleozoic metamorphics in Palawan (the Philippines)? Evidence from single grain U-Pb dating of detrital zircons. *Journal of Asian Earth Sciences*, *52*, 134–145. https://doi.org/10.1016/j.jseaes.2012.03.005

Waldron, J. W., & van Staal, C. R. (2001). Taconian orogeny and the accretion of the Dashwoods block: A peri-Laurentian microcontinent in the Iapetus Ocean. *Geology*, *29*(9), 811–814. https://doi.org/10.1130/0091-7613(2001)029<0811:TOATAO>2.0.CO;2

Wang, P. (2012). Tracing the life history of a marginal sea—On "The South China Sea Deep" research program. *Chinese Science Bulletin*, *57*(24), 3093–3114. https://doi.org/10.1007/s11434-012-5087-1

Wang, P., Jian, Z., Zhao, Q., Li, Q., Wang, R., Liu, Z., et al. (2003). Evolution of the South China Sea and monsoon history revealed in deep-sea records. *Chinese Science Bulletin*, *48*(23), 2549–2561. https://doi.org/10.1360/03wd0156

Wang, P., Prell, W. L., & Blum, P. (2000). *Proceedings of the Ocean Drilling Program, Initial Reports*. (Vol. 184). College Station, TX: Ocean Drilling Program. https://doi.org/10.2973/odp.proc.ir.184.2000

Wang, W., Yang, X., Bidgoli, T. S., & Ye, J. (2019). Detrital zircon geochronology reveals source-to-sink relationships in the Pearl River Mouth Basin, China. *Sedimentary Geology, 388, 81–98*. https://doi.org/10.1016/j.sedgeo.2019.04.004

Wang, W., Ye, J., Bidgoli, T., Yang, X., Shi, H., & Shu, Y. (2017). Using detrital zircon geochronology to constrain Paleogene provenance and its relationship to rifting in the Zhu 1 depression, Pearl River Mouth Basin, South China Sea. *Geochemistry, Geophysics, Geosystems*, *18*(11), 3976–3999. https://doi.org/10.1002/2017GC007110

Wang, W., Yang, X., Bidgoli, T. S., & Ye, J. (2019). Detrital zircon geochronology reveals source-to-sink relationships in the Pearl River Mouth Basin, China. *Sedimentary geology*, *388*, 81–98. https://doi.org/10.1016/j.sedgeo.2019.04.004

Wei, G. J., Liang, X. R., Li, X. H., & Liu, Y. (2002). Precise measurement of Sr isotopic composition of liquid and solid base using (LP)MC-ICPMS. *Geochimica*, *31* (3), 295–299 (in Chinese with English abstract). https://doi.org/10.1080/12265080208422884

Wiedenbeck, M., Hanchar, J. M., Peck, W. H., Sylvester, P., Valley, J., Whitehouse, M., et al. (2004). Further characterisation of the 91500 zircon crystal. *Geostandards and Geoanalytical Research*, *28*(1), 9-39. https://doi.org/10.1111/j.1751-908X.2004.tb01041.x

Wolfart, R., Čepek, P., Gramann, F., Kemper, E., & Porth, H. (1986). Stratigraphy of Palawan Island, Philippines. *Newsletters on Stratigraphy*, *16*(1), 19–48.

Xie, H., Zhou, D., Li, Y., Pang, X., Li, P., Chen, G., Li, F., & Cao, J. (2014). Cenozoic tectonic subsidence in deepwater sags in the Pearl River Mouth Basin, northern South China Sea. *Tectonophysics*, *615*, 182–198. https://doi.org/10.1016/j.tecto.2014.01.010

Xu, C. H., Shi, H. S., Barnes, C. G., & Zhou, Z. Y. (2016). Tracing a late Mesozoic magmatic arc along the Southeast Asian margin from the granitoids drilled from the northern South China Sea. *International Geology Review*, *58* (1), 71–94.

Xu, X., O'Reilly, S. Y., Griffin, W. L., Wang, X., Pearson, N. J., & He, Z. (2007). The crust of Cathaysia: age, assembly and reworking of two terranes. *Precambrian Research*, *158*(1–2), 51–78. https://doi.org/10.1016/j.precamres.2007.04.010

Yan, Y., Yao, D., Tian, Z., Huang, C., Chen, W., Santosh, M., Yumul Jr., G. P., Dimalanta, C. B., & Li, Z. (2018). Zircon U-Pb chronology and Hf isotope from the Palawan-Mindoro Block, Philippines: Implication to provenance and tectonic evolution of the South China Sea. *Tectonics*, *37*(4), 1063–1076. https://doi.org/10.1002/2017TC004942

Yang, F. L., Gao, D., Sun, Z., Zhou, Z. Y., Wu, Z., & Li, Q. Y. (2012). The evolution of the South China Sea Basin in the Mesozoic-Cenozoic and its significance for oil and gas exploration: A review and overview. In D. Gao (Eds.), *Tectonics and sedimentation: Implications for petroleum systems*, *AAPG Memoir* (Vol. 100, pp. 397–418). https://doi.org/10.1306/13351562M1003528

Yao, Y., Liu, H., Yang, C., Han, B., Tian, J., Yin, Z., Gong, J., & Xu, Q. (2012). Characteristics and evolution of Cenozoic sediments in the Liyue Basin, SE South China Sea. *Journal of Asian Earth Sciences*, *60*, 114–129. https://doi.org/10.1016/j.jseaes.2012.08.003

Ye, Q., Mei, L., Shi, H., Camanni, G., Shu, Y., Wu, J., Deng, P. & Li, G. (2018). The Late Cretaceous tectonic evolution of the South China Sea area: An overview, and new

perspectives from 3D seismic reflection data. Earth-Science Reviews, 187, 186–204. https://doi.org/10.1016/j.earscirev.2018.09.013

Yu, J. H., Wei, Z. Y., Wang, L. J., Shu, L. S., & Sun, T. (2006). Cathaysia Block: a young continent composed of ancient materials. *Geological Journal of China Universities*, *12*(4), 440–447. https://doi.org/10.3969/j.issn.1006-7493.2006.04.004

Yumul Jr., G. P., Dimalanta, C. B., Tamayo, R. A., & Maury, R. C. (2003). Collision, subduction and accretion events in the Philippines: a synthesis. Island Arc, *12*(2), 77–91. https://doi.org/10.1046/j.1440-1738.2003.00382.x

Yumul Jr., G. P., Dimalanta, C. B., Marquez, E. J., & Queaño, K. L. (2009). Onland signatures of the Palawan microcontinental block and Philippine mobile belt collision and crustal growth process: a review. *Journal of Asian Earth Sciences*, *34*, 610–623. https://doi.org/10.1016/j.jseaes.2008.10.002

Zamoras, L. R., & Matsuoka, A. (2004). Accretion and postaccretion tectonics of the Calamian Islands, North Palawan block, Philippines. *Island Arc*, *13*(4), 506–519. https://doi.org/10.1111/j.1440-1738.2004.00443.x

Zhao, M., Shao, L., & Qiao, P. J. (2015). Characteristics of detrital zircon U-Pb geochronology of the Pearl River sands and its implication on provenances [in Chinese with English abstract]. *Journal of Tongji University*, *43*, 915–923. https://doi.org/10.11908/j.issn.0253-374x.2015.06.018

Zhou, D., Ru, K., & Chen, H. Z. (1995). Kinematics of Cenozoic extension on the South China Sea continental margin and its implications for the tectonic evolution of the region. *Tectonophysics*, *251*, 161–177. http://dx.doi.org/10.1016/0040-1951(95)00018-6.

Figure Captions

Figure 1. Geological map of Southeast Asia surrounding the South China Sea adapted from Yan et al. (2018). The boundary of the Palawan microcontinental block outlined with red dashed line was modified from Liu et al. (2014). The shaded areas in the rifting basins on the South China margin represent the structural depressions. Also shown are the ocean drilling sites and industrial boreholes referred to in the text. In the Pearl River Mouth Basin, boreholes drilling the Eocene syn-rift sediments (Shao et al., 2016, 2019) are marked by green diamond. For the wells offshore Palawan: A-1=Anepahan-1; P-1=Penascosa-1; B-1=Busuanga-1. JSF=Jiangshao Fault Zone; RI= Romblon Islands.

Figure 2. (a) Simplified geological map of Palawan Island adapted from Yumul et al. (2009). (b) Geological map of central-southern Palawan (Aurelio et al., 2014) showing the sampling sites of the Panas-Pandian Formation. The sample names in italics denote sandstone samples, while the rest represent mudstone samples.

Figure 3. Field photographs of outcrops of the Panas-Pandian Formation. (a) Grey-greenish massive sandstone at Site RZ-01, showing a clear graded bedding from coarse- to medium-grained sandstone upwards. The arrow (scale) has a length of 10 cm. (b) Alternations of medium- to thick-bedded sandstone and thin-bedded mudstone that are highly weathered, at Site RZ-04. (c) Interbeds of light-grey thin-bedded sandstone and medium- to thick-bedded mudstone at Site RZ-12. (d) Trace fossil *Helminthopsis* well preserved in convex hyporelief on sandstone soles at Site RZ-12. (e) Highly indurated medium- to thick-bedded sandstone and thin-bedded shale interbeds at Site AB-02. (f) Sandstone bed at Site AB-02 with parallel bedding.

Figure 4. Datum planes of age-diagnostic microfossils in the Lichi Mélange. Datum planes of planktonic foraminifers and calcareous nannofossils are given according to Wade et al. (2011) and Anthonissen and Ogg (2012), respectively. Both the age spans derived from this study and Wolfart et al. (1984) are shown.

Figure 5. (a) SEM images of planktonic foraminifers recovered from the Panas-Pandian Formation are shown with scale bars of 200 μm. Numbers 1–8 recovered from Sample RZ-12c: 1–2. *Acarinina bullbrooki* (Bolli); 3–4. *Acarinina cuneicamerata* (Blow); 5–7. *Morozovelloides crassatus* (Cushman); 8. *Globigerinatheka subconglobata* (Shutskaya). 9. *Globigerinatheka subconglobata* (Shutskaya), Sample RZ-12; 10. *Cataphydrax unicavus* Bolli, Loeblich and Tappan, Sample RZ-12a. (b) Polarizing photographs of calcareous nannofossil recovered from the Panas-Pandian Formation are shown with their approximate diameter of the fossil (red bar). Numbers 1–6 recovered from Sample RZ-12: 1. *Discoaster lodoensis* Bramlette and Riedel; 2. *Discoaster kupperi* Stradner; 3. *Discoaster saipanensis* Bramlette and Riedel; 4. *Nannotetrina cristata* (Martini); 5. *Discoaster barbadiensis* Tan; 6. *Discoaster gemmifer* Stradner. Numbers 7–11 recovered from Sample RZ-12a: 7. *Discoaster lodoensis* Bramlette and Riedel; 8. *Discoaster kupperi* Stradner; 9. *Sphenolithus spiniger* Bukry; 10. *Sphenolithus moriformis* (Brönnimann and Stradner); 11. *Ericsonia formosa* (Kamptner). Numbers 12–16 recovered from Sample RZ-12c: 12. *Discoaster lodoensis*

Bramlette and Riedel; 13. *Discoaster kupperi* Stradner; 14. *Discoaster saipanensis* Bramlette and Riedel; 15. *Discoaster barbadiensis* Tan; 16. *Discoaster deflandrei* Bramlette and Riedel. (c) Composite all-in-focus stereomicroscopic images of benthic foraminifers recovered from the Panas-Pandian Formation are shown with scale bars of 200 μm. 1. *Haplophragmoides eggeri* Cushman, Sample-03b. Numbers 2–3 recovered from RZ-03d: 2. *Psammosphaera irregularis* Grzybowski; 3. *Reticulophragmium amplectens* (Grzybowski). Numbers 4–10 recovered from Sample RZ-04b: 4. *Haplophragmoides walteri* (Grzybowski); 5. *Psammosphaera irregularis* Grzybowski; 6–7. *Pseudonodosinella elongata* (Grzybowski); 8. *Saccammina grzybowskii* (Schubert); 9–10. *Trochamminna globigeriniformis* (Parker and Jones). 11. *Psammosiphonella discreta* (Brady), Sample RZ-04c. Numbers 12–19 recovered from Sample RZ-05c: 12. *Ammodiscus tenuissimus* Grzybowski; 13. *Haplophragmium horridum* Grzybowski; 14–15. *Haplophragmoides walteri* (Grzybowski); 16. *Nothia excelsa* (Grzybowski); 17. *Psammosphaera irregularis* Grzybowski; 18. *Trochamminna globigeriniformis* (Parker and Jones); 19. *Trochamminoides subcoronatus* (Grzybowski). 20. *Haplophragmoides walteri* (Grzybowski), Sample RZ-07. Numbers 21–23 recovered from RZ-12: 21. *Cibicides* sp.; 22. *Lenticulina* sp.; 23. *Planulina* sp.. 24. *Pseudonodosaria* sp., Sample RZ-12c.

Figure 6. (a) Upper continental crust (UCC) (Rudnick & Gao, 2003) normalized multi-trace element diagram for the Panas-Pandian Formation mudstones, as compared with the Middle–Late Eocene sediments from Site U1435 and borehole L21 (Shao, Meng, et al., 2017). (b) Chondrite-normalized REE distribution plot for the Panas-Pandian Formation mudstones as compared with the UCC and the Middle–Late Eocene sediments from Site U1435 and borehole L21 (Shao, Meng, et al., 2017). The chondrite values are cited from Sun and McDonough (1989).

Figure 7. Heavy mineral assemblage from the Panas-Pandian Formation sandstones, as compared with the average of results published by Shao, Cao, et al. (2017) (see location of their six samples in Figure 2b).

Figure 8. Comparison of U-Pb age spectra for detrital zircon from (a-e) the Panas-Pandian Formation (this study, Shao, Cao, et al., 2017; Yan et al., 2018), (f) the modern sediments of the northeastern tributaries of the Pearl River (Liu et al., 2017; Xu et al., 2007; Zhao et al., 2015), (g) the Middle–Late Eocene sediments of the boreholes in the Pearl River Mouth

Basin (Shao et al., 2016, 2019; Wang et al., 2017), and (h) the Middle–Late Eocene sediments of Site U1435 (Shao, Meng, et al., 2017).

Figure 9. Simplified stratigraphic column for the Cenozoic sediments in central-southern Palawan showing the timing of the breakup unconformity at 33–32 Ma, as compared with the breakup unconformity of the northern margin of the South China Sea (Chen et al., 2003; Huang et al., 2013, 2017; Li et al., 2017; Xie et al., 2014; Zhou et al., 1995).

Figure 10. Plots of (a) Cr/V vs Y/Ni and (b) Co/Th vs La/Sc and ternary plots of (c) La-Th-Sc and (d) Th-Sc-Zr/10 of the Panas-Pandian Formation mudstones, as compared with the Middle–Late Eocene sediments from Site U1435 and borehole L21 (Shao, Meng, et al., 2017). (e) Relative probability plot of Nd isotope compositional ranges of the Panas-Pandian Formation mudstones. Also shown are those of the Cathaysia Block, the Yangtze Block and the Indochina Block (Clift et al., 2006 and references therein).

Figure 11. Nonmetric multidimensional scaling (MDS**)** map (Vermeesch et al., 2013) for detrital zircon U-Pb ages of the Panas-Pandian Formation (this study and Yan et al. 2018, black circles; Shao, Cao, et al., 2017, orange circles), the Middle–Late Eocene sediments of the boreholes in the Pearl River Mouth Basin (Shao et al., 2016, 2019) (green diamonds), the Middle–Late Eocene sediments of Site U1435 (Shao, Meng, et al., 2017) and the modern sediments of the northeastern tributaries of the Pearl River (NEPR) (Xu et al., 2007; Zhao et al., 2015; Liu et al., 2017). The Kolmogorov-Smirnov effect size is used as the measure of dissimilarity. The stress value is 0.035, indicating an excellent goodness-of-fit. Solid and dashed lines in the map indicate the closest and second closest neighbors, respectively.

Figure 12. Paleogeographic reconstruction for the South China margin during the Middle Eocene (47.7–42.1 Ma) (revised from Hall, 2002; Li et al., 2017), showing two source regions for the Panas-Pandian Formation, a distant source from the interior Cataysia Block and a proximal source from the Mesozoic basement uplift. The inferred Middle Eocene coastline is mainly based on Huang et al. (2019), Li et al (2017) and Yao et al. (2012). PRMB=Pearl River Mouth Basin; QDNB=Qiongdongnan Basin; TXNB=Taixinan Basin; RB=Reed Bank; MB=Macclesfield Bank.

Tables

Table 1 εNd values of the mudstone of the Panas-Pandian Formation.

Sample No.	$^{143}Nd/^{144}Nd$	SE	εNd
RZ-03b	0.512177	0.000004	-9.0
RZ-04b	0.512214	0.000005	-8.3
RZ-05a	0.512192	0.000004	-8.7
RZ-06c	0.512207	0.000004	-8.4
RZ-08	0.512209	0.000005	-8.4
RZ-12	0.512180	0.000005	-8.9
RZ-12a	0.512185	0.000005	-8.8
RZ-12c	0.512181	0.000004	-8.9
RZ-13a	0.512210	0.000004	-8.3
AB-02a	0.512162	0.000005	-9.3
AB-02b	0.512169	0.000006	-9.2
Average			***-8.7***

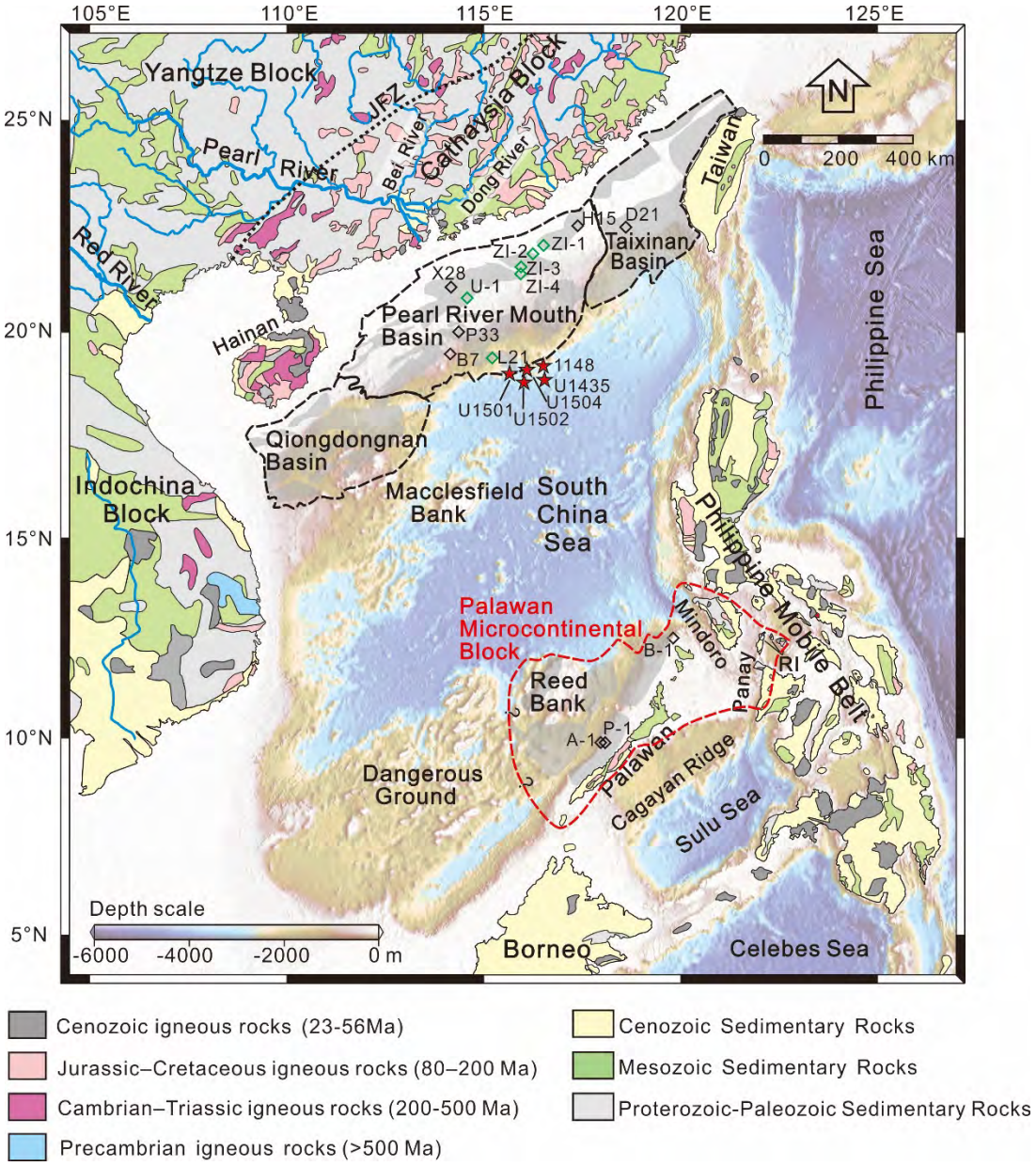
105°E
110°E
115°E
120°E
125°E
25°N
20°N
15°N
10°N
5°N
Yangtze Block
JFZ
Cathaysia Block
Pearl River
Bei River
Dong River
Red River
Taiwan
N
0
200
400 km
H15
D21
Taixinan Basin
ZI-2
ZI-1
ZI-3
ZI-4
X28
U-1
Pearl River Mouth Basin
P33
B7
L21
1148
U1435
U1504
U1501
U1502
Hainan
Qiongdongnan Basin
Indochina Block
Macclesfield Bank
South China Sea
Philippine Sea
Philippine Mobile Belt
Palawan Microcontinental Block
Mindoro
B-1
RI
Panay
Reed Bank
A-1
P-1
Palawan
Cagayan Ridge
Dangerous Ground
Sulu Sea
Depth scale
-6000
-4000
-2000
0 m
Borneo
Celebes Sea
Cenozoic igneous rocks (23-56Ma)
Jurassic–Cretaceous igneous rocks (80–200 Ma)
Cambrian–Triassic igneous rocks (200-500 Ma)
Precambrian igneous rocks (>500 Ma)
Cenozoic Sedimentary Rocks
Mesozoic Sedimentary Rocks
Proterozoic-Paleozoic Sedimentary Rocks

Figure 1

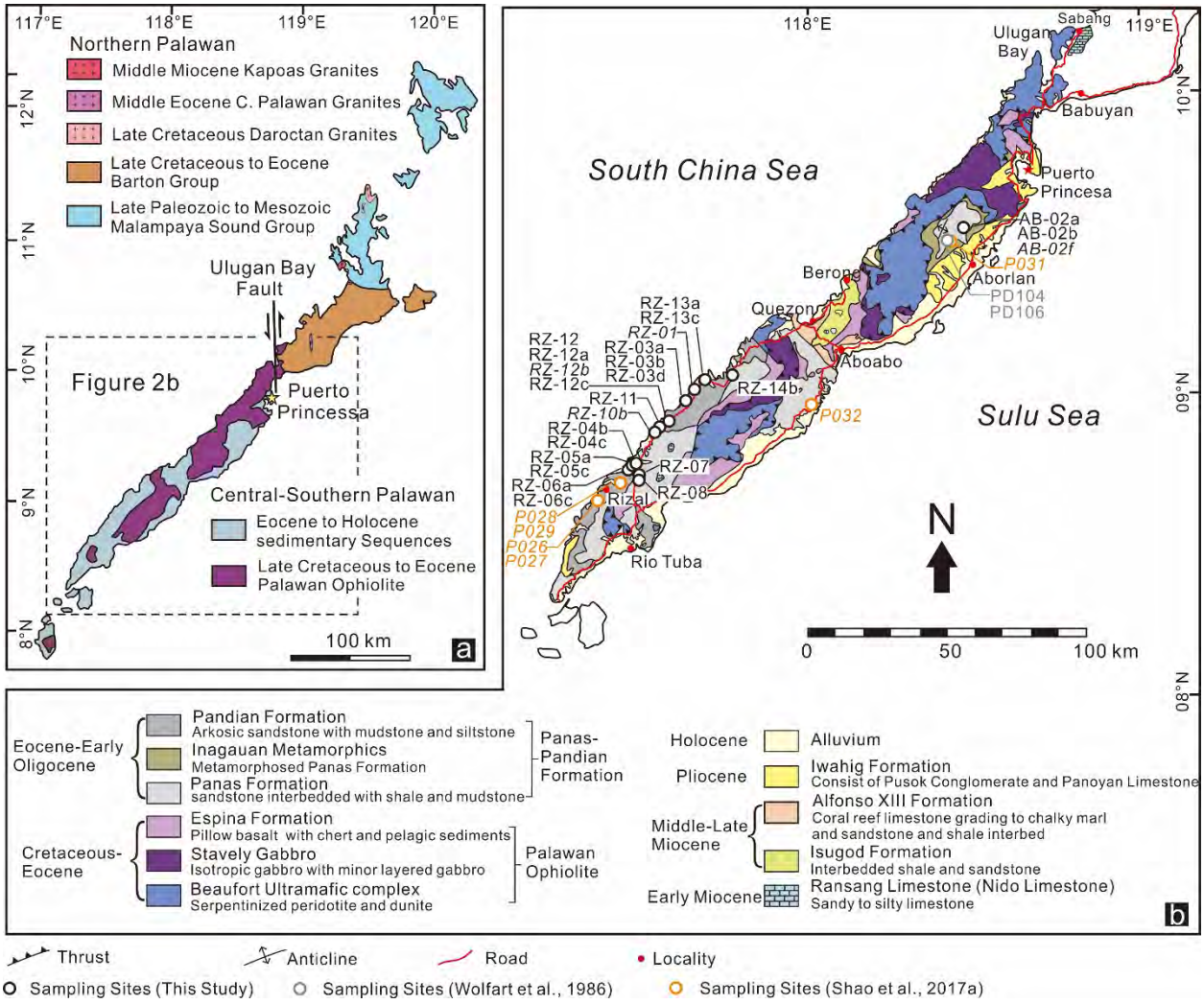
117°E
118°E
119°E
120°E
12°N
11°N
10°N
9°N
8°N
Northern Palawan
Middle Miocene Kapoas Granites
Middle Eocene C. Palawan Granites
Late Cretaceous Daroctan Granites
Late Cretaceous to Eocene Barton Group
Late Paleozoic to Mesozoic Malampaya Sound Group
Ulugan Bay Fault
Figure 2b
Puerto Princessa
Central-Southern Palawan
Eocene to Holocene sedimentary Sequences
Late Cretaceous to Eocene Palawan Ophiolite
100 km
a
South China Sea
Sulu Sea
Ulugan Bay
Sabang
Babuyan
Puerto Princesa
AB-02a
AB-02b
AB-02f
P031
Aborlan
PD104
PD106
Berong
Quezon
Aboabo
RZ-14b
P032
RZ-13a
RZ-13c
RZ-01
RZ-12
RZ-12a
RZ-12b
RZ-12c
RZ-03a
RZ-03b
RZ-03d
RZ-11
RZ-10b
RZ-04b
RZ-04c
RZ-05a
RZ-05c
RZ-06a
RZ-06c
RZ-07
RZ-08
Rizal
P028
P029
P026
P027
Rio Tuba
N
0
50
100 km
Eocene-Early Oligocene
Pandian Formation
Arkosic sandstone with mudstone and siltstone
Inagauan Metamorphics
Metamorphosed Panas Formation
Panas Formation
sandstone interbedded with shale and mudstone
Panas-Pandian Formation
Cretaceous-Eocene
Espina Formation
Pillow basalt with chert and pelagic sediments
Stavely Gabbro
Isotropic gabbro with minor layered gabbro
Beaufort Ultramafic complex
Serpentinized peridotite and dunite
Palawan Ophiolite
Holocene
Alluvium
Pliocene
Iwahig Formation
Consist of Pusok Conglomerate and Panoyan Limestone
Middle-Late Miocene
Alfonso XIII Formation
Coral reef limestone grading to chalky marl and sandstone and shale interbed
Isugod Formation
Interbedded shale and sandstone
Early Miocene
Ransang Limestone (Nido Limestone)
Sandy to silty limestone
b
Thrust
Anticline
Road
Locality
Sampling Sites (This Study)
Sampling Sites (Wolfart et al., 1986)
Sampling Sites (Shao et al., 2017a)

Figure 2

Figure 3

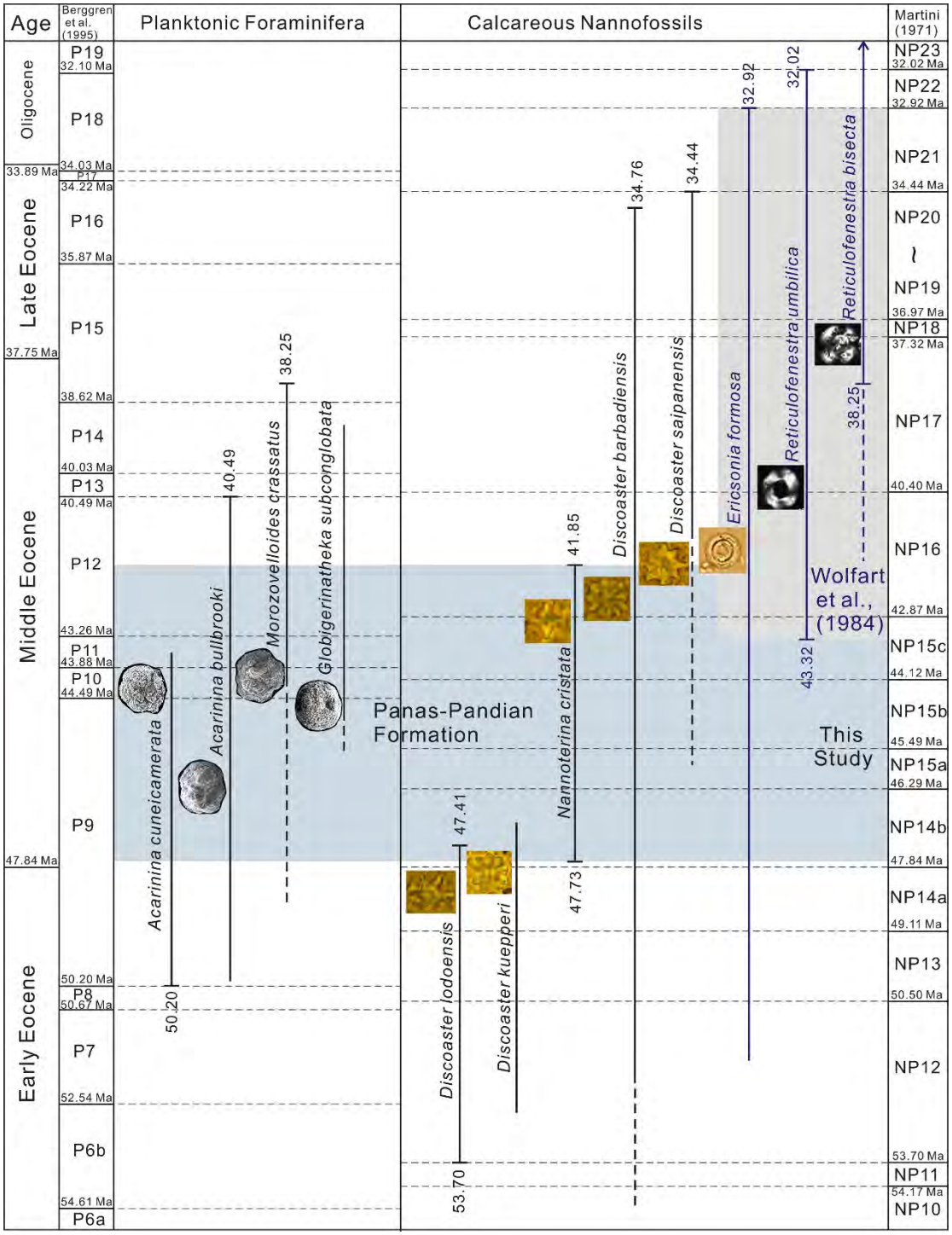
Age
Berggren et al. (1995)
Planktonic Foraminifera
Calcareous Nannofossils
Martini (1971)
Oligocene
Late Eocene
Middle Eocene
Early Eocene
P19
32.10 Ma
P18
34.03 Ma
P17
34.22 Ma
P16
35.87 Ma
P15
38.62 Ma
P14
40.03 Ma
P13
40.49 Ma
P12
43.26 Ma
P11
43.88 Ma
P10
44.49 Ma
P9
47.84 Ma
P8
50.67 Ma
P7
52.54 Ma
P6b
54.61 Ma
P6a
33.89 Ma
37.75 Ma
50.20 Ma
NP23
32.02 Ma
NP22
32.92 Ma
NP21
34.44 Ma
NP20
NP19
36.97 Ma
NP18
37.32 Ma
NP17
40.40 Ma
NP16
42.87 Ma
NP15c
44.12 Ma
NP15b
45.49 Ma
NP15a
46.29 Ma
NP14b
47.84 Ma
NP14a
49.11 Ma
NP13
50.50 Ma
NP12
53.70 Ma
NP11
54.17 Ma
NP10
Acarinina cuneicamerata
Acarinina bullbrooki
Morozovelloides crassatus
Globigerinatheka subconglobata
50.20
40.49
38.25
Panas-Pandian Formation
Discoaster lodoensis
Discoaster kuepperi
Nannoterina cristata
Discoaster barbadiensis
Discoaster saipanensis
Ericsonia formosa
Reticulofenestra umbilica
Reticulofenestra bisecta
53.70
47.41
47.73
41.85
34.76
34.44
32.92
32.02
38.25
43.32
Wolfart et al., (1984)
This Study

Figure 4

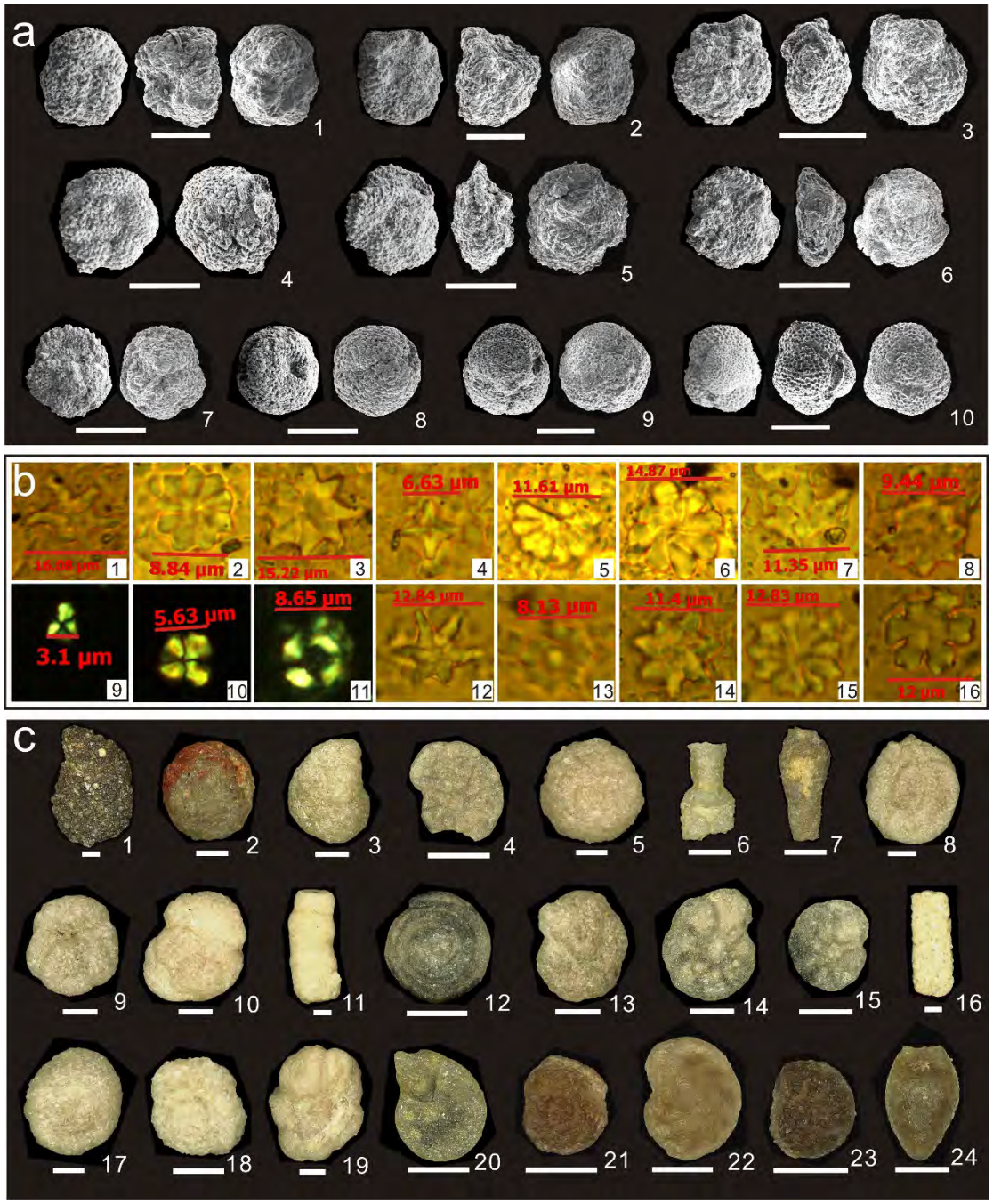
a
1
2
3
4
5
6
7
8
9
10
b
8.84 µm
6.63 µm
11.61 µm
11.35 µm
9.44 µm
3.1 µm
5.63 µm
8.65 µm
c

Figure 5

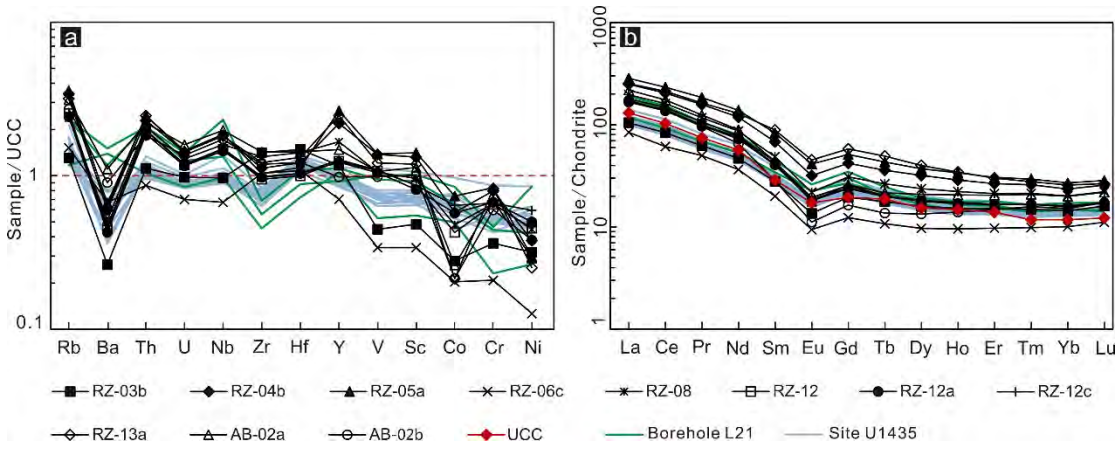
a
b
Sample/UCC
Sample/Chondrite
0.1
1
10
100
1000
Rb Ba Th U Nb Zr Hf Y V Sc Co Cr Ni
La Ce Pr Nd Sm Eu Gd Tb Dy Ho Er Tm Yb Lu
RZ-03b
RZ-04b
RZ-05a
RZ-06c
RZ-08
RZ-12
RZ-12a
RZ-12c
RZ-13a
AB-02a
AB-02b
UCC
Borehole L21
Site U1435

Figure 6

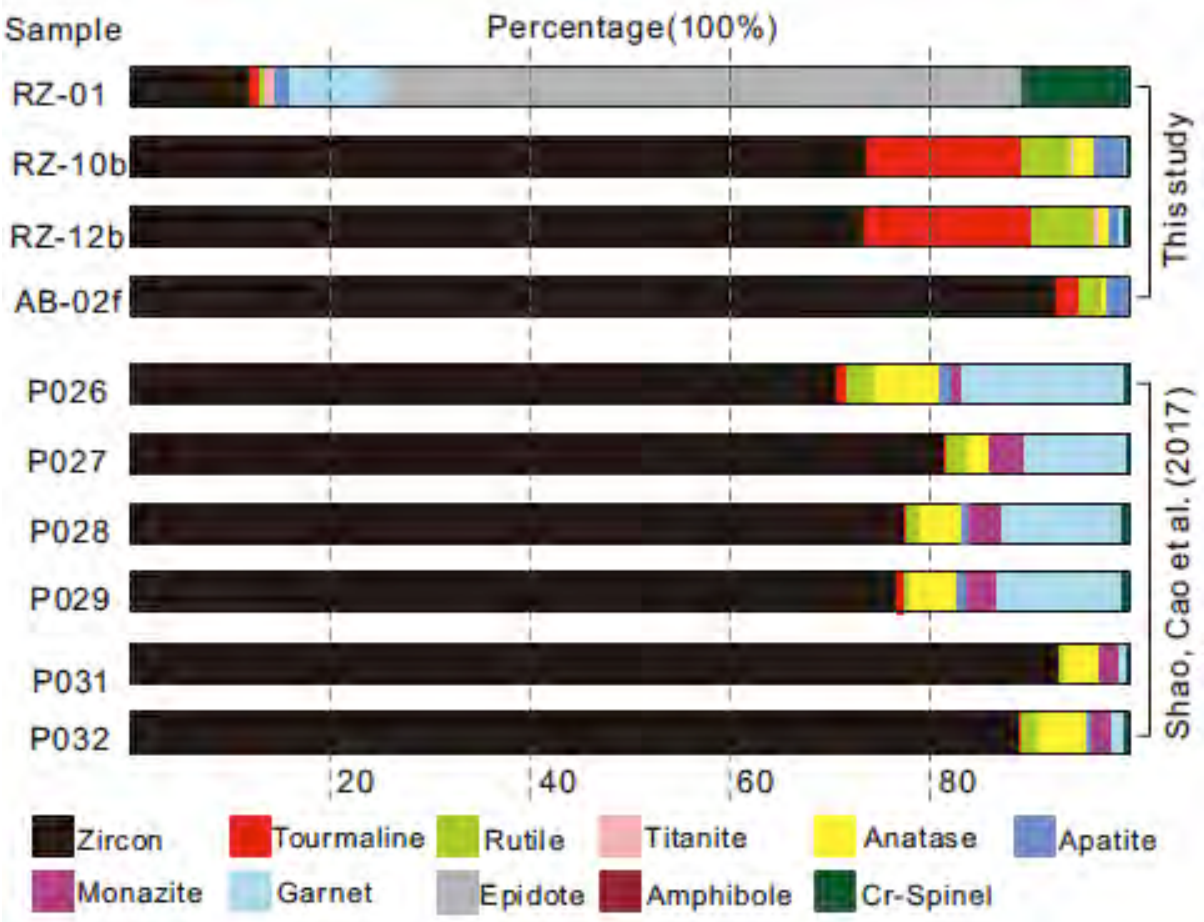
Sample
Percentage(100%)
RZ-01
RZ-10b
RZ-12b
AB-02f
P026
P027
P028
P029
P031
P032
This study
Shao, Cao et al. (2017)
20
40
60
80
Zircon
Tourmaline
Rutile
Titanite
Anatase
Apatite
Monazite
Garnet
Epidote
Amphibole
Cr-Spinel

Figure 7

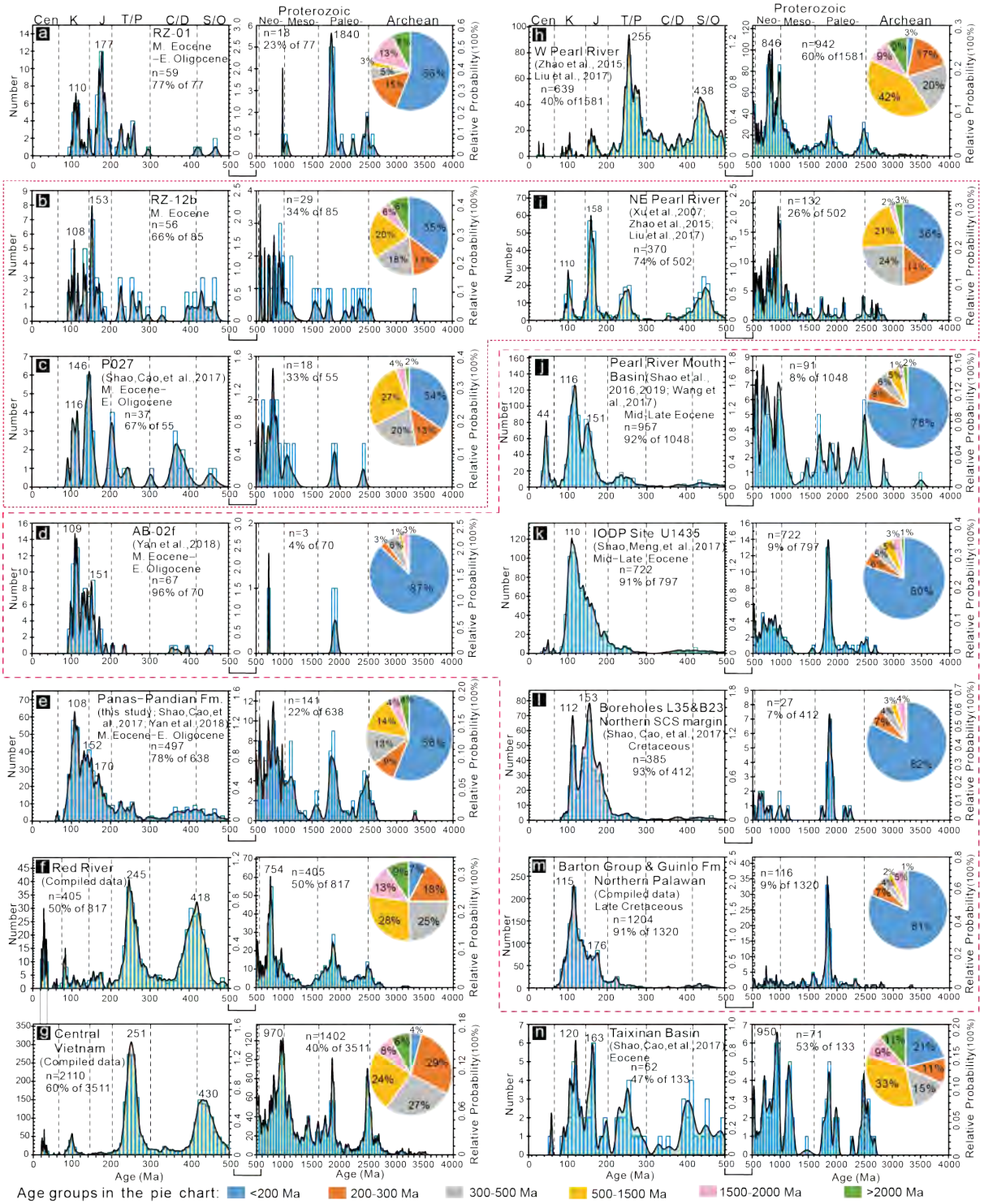
a RZ-01
M. Eocene –E. Oligocene
n=59
77% of 77
b RZ-12b
M. Eocene
n=56
66% of 85
c P027
(Shao,Cao,et al.,2017)
M. Eocene–E. Oligocene
n=37
67% of 55
d AB-02f
(Yan et al.,2018)
M. Eocene–E. Oligocene
n=67
96% of 70
e Panas-Pandian Fm.
(this study; Shao,Cao,et al.,2017; Yan et al.,2018)
M. Eocene–E. Oligocene
n=497
78% of 638
f Red River
(Compiled data)
n=405
50% of 817
g Central Vietnam
(Compiled data)
n=2110
60% of 3511
h W Pearl River
(Zhao et al.,2015; Liu et al.,2017)
n=639
40% of 1581
i NE Pearl River
(Xu et al.,2007; Zhao et al.,2015; Liu et al.,2017)
n=370
74% of 502
j Pearl River Mouth Basin
(Shao et al.,2016,2019; Wang et al.,2017)
Mid-Late Eocene
n=957
92% of 1048
k IODP Site U1435
(Shao,Meng et al.,2017)
Mid-Late Eocene
n=722
91% of 797
l Boreholes L35&B23
Northern SCS margin
(Shao,Cao,et al.,2017)
Cretaceous
n=385
93% of 412
m Barton Group & Guinlo Fm
Northern Palawan
(Compiled data)
Late Cretaceous
n=1204
91% of 1320
n Taixinan Basin
(Shao,Cao,et al.,2017)
Eocene
n=62
47% of 133
Cen K J T/P C/D S/O
Proterozoic
Neo- Meso- Paleo-
Archean
Number
Relative Probability(100%)
Age (Ma)
Age groups in the pie chart: <200 Ma 200-300 Ma 300-500 Ma 500-1500 Ma 1500-2000 Ma >2000 Ma

Figure 8

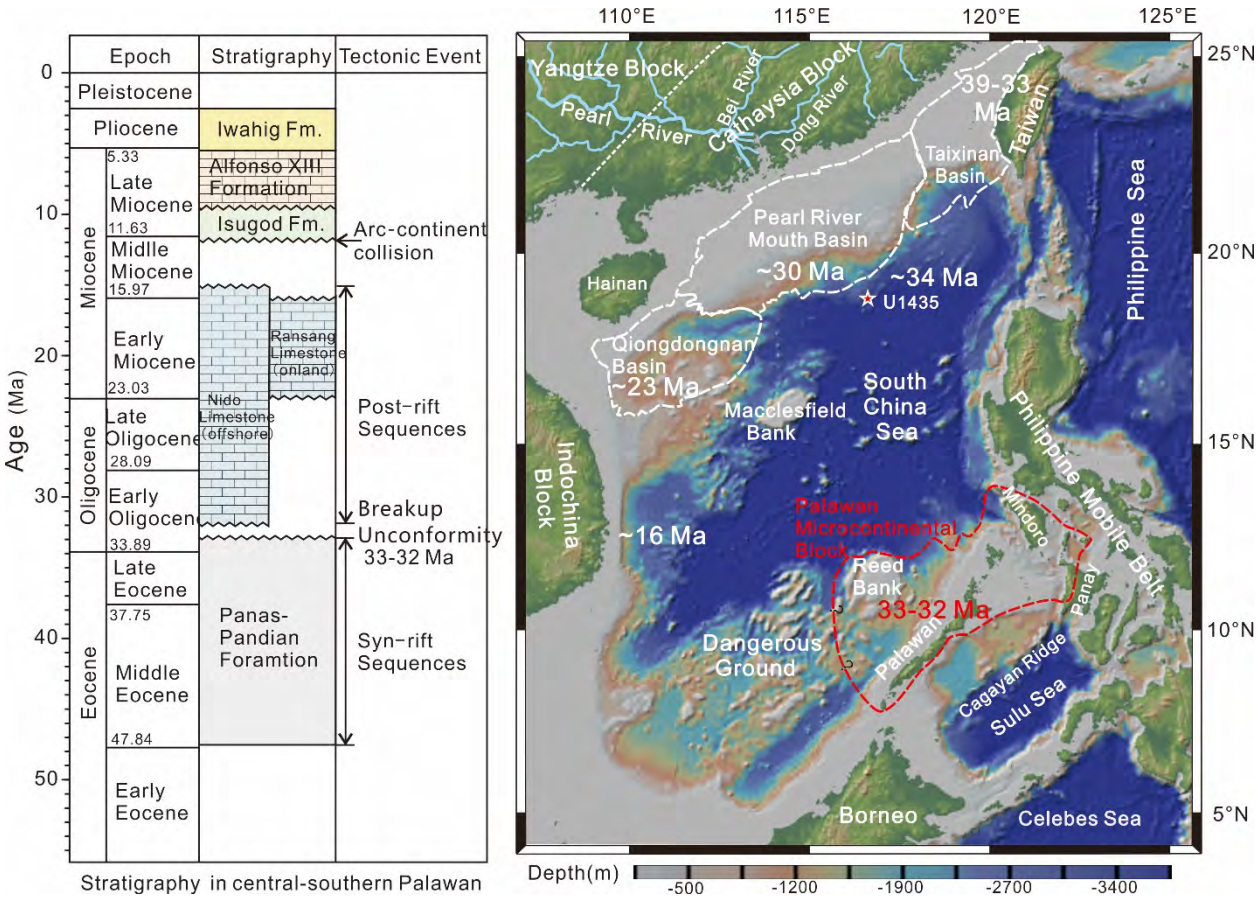
Epoch
Stratigraphy
Tectonic Event
Age (Ma)
Pleistocene
Pliocene
Iwahig Fm.
5.33
Late Miocene
Alfonso XIII Formation
11.63
Isugod Fm.
Arc-continent collision
Midlle Miocene
15.97
Early Miocene
Ransang Limestone (onland)
23.03
Nido Limestone (offshore)
Late Oligocene
Post-rift Sequences
28.09
Early Oligocen
Breakup Unconformity 33-32 Ma
33.89
Late Eocene
37.75
Panas-Pandian Foramtion
Middle Eocene
Syn-rift Sequences
47.84
Early Eocene
Miocene
Oligocene
Eocene
Stratigraphy in central-southern Palawan
110°E
115°E
120°E
125°E
25°N
20°N
15°N
10°N
5°N
Yangtze Block
Pearl River
Bei River
Cathaysia Block
Dong River
39-33 Ma
Taiwan
Taixinan Basin
Philippine Sea
Pearl River Mouth Basin
~30 Ma
~34 Ma
U1435
Hainan
Qiongdongnan Basin
~23 Ma
Macclesfield Bank
South China Sea
Philippine Mobile Belt
Indochina Block
~16 Ma
Palawan Microcontinental Block
Mindoro
Reed Bank
33-32 Ma
Panay
Dangerous Ground
Palawan
Cagayan Ridge
Sulu Sea
Borneo
Celebes Sea
Depth(m)
-500
-1200
-1900
-2700
-3400

Figure 9

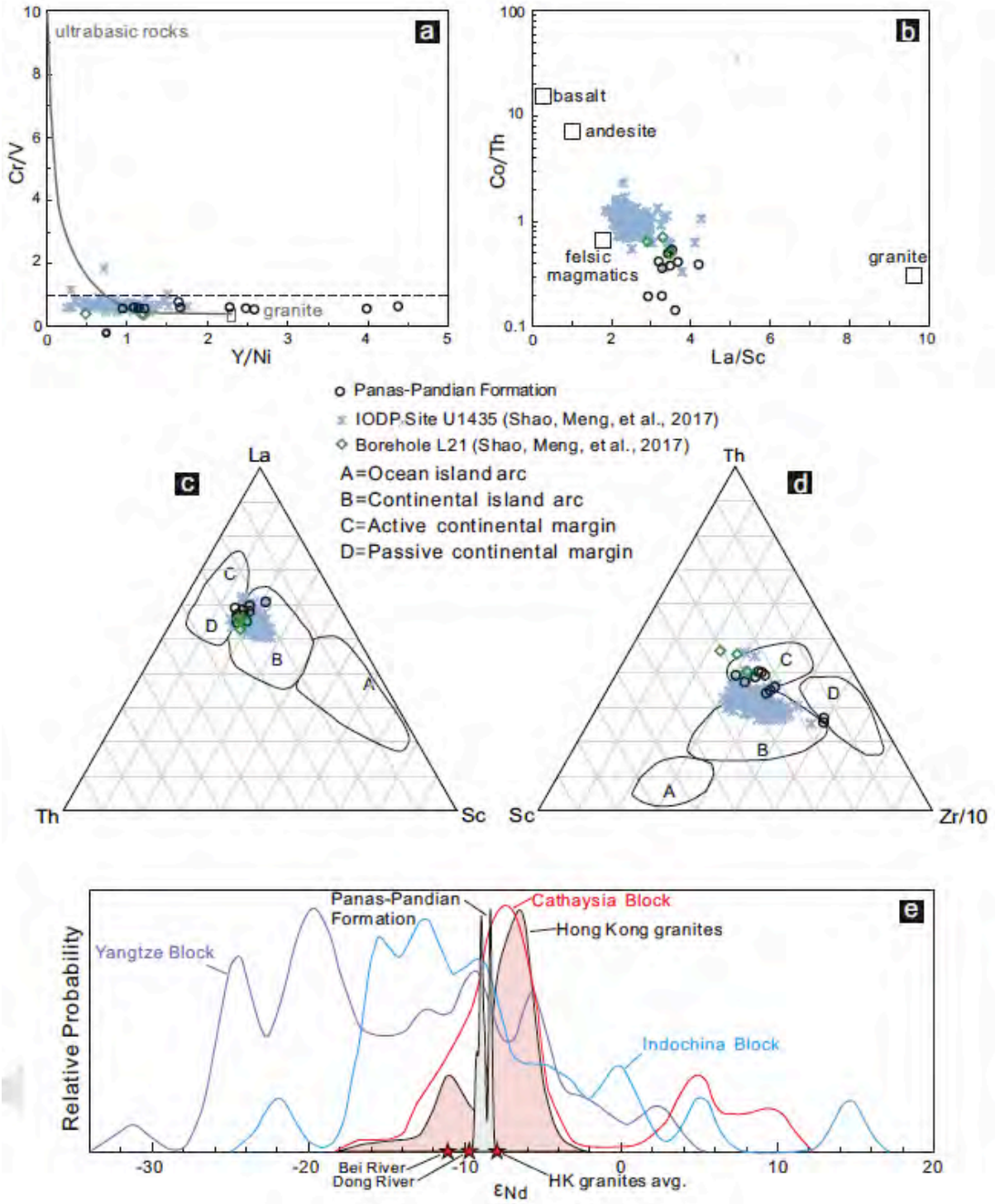
a
ultrabasic rocks
granite
Cr/V
Y/Ni
b
basalt
andesite
felsic magmatics
granite
Co/Th
La/Sc
Panas-Pandian Formation
IODP Site U1435 (Shao, Meng, et al., 2017)
Borehole L21 (Shao, Meng, et al., 2017)
A=Ocean island arc
B=Continental island arc
C=Active continental margin
D=Passive continental margin
c
La
Th
Sc
d
Th
Sc
Zr/10
e
Relative Probability
Panas-Pandian Formation
Cathaysia Block
Hong Kong granites
Yangtze Block
Indochina Block
Bei River
Dong River
HK granites avg.
εNd

Figure 10

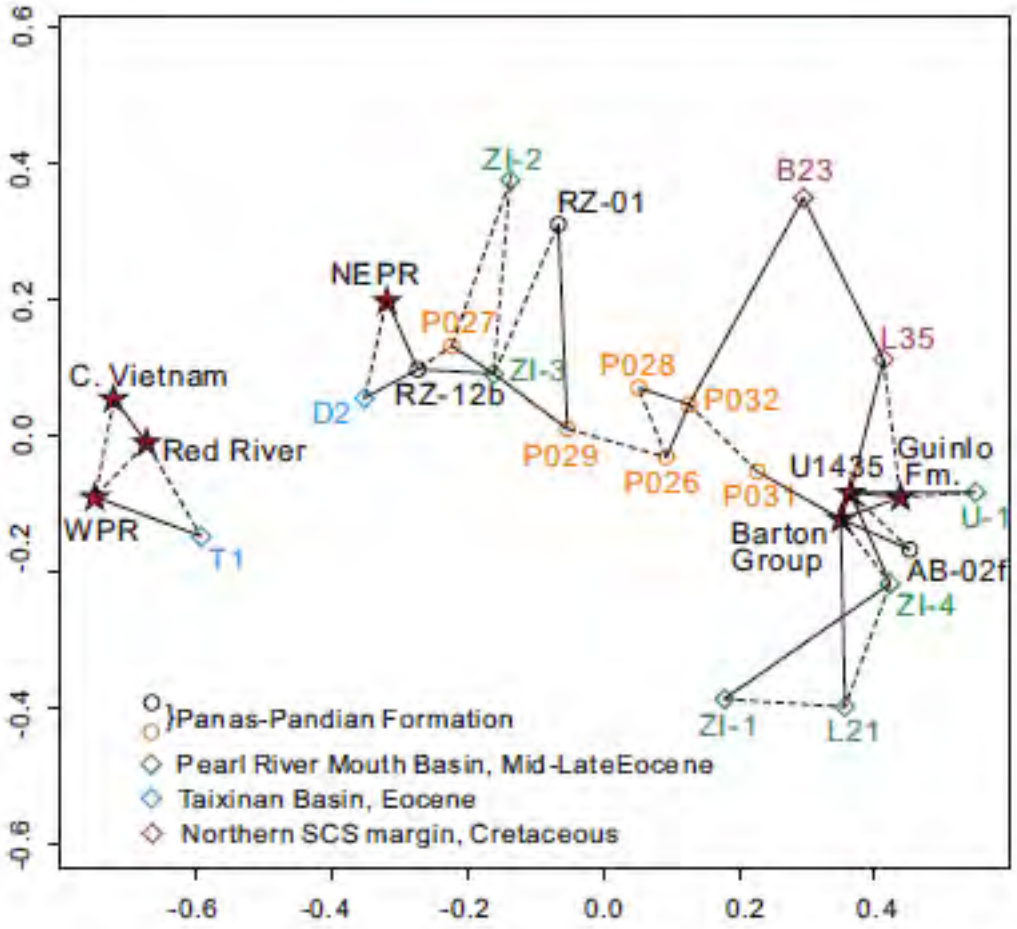
ZI-2
RZ-01
B23
NEPR
P027
L35
P028
ZI-3
C. Vietnam
RZ-12b
P032
D2
Red River
P029
P026
U1435
Guinlo Fm.
P031
U-1
WPR
T1
Barton Group
AB-02f
ZI-4
Panas-Pandian Formation
ZI-1
L21
Pearl River Mouth Basin, Mid-LateEocene
Taixinan Basin, Eocene
Northern SCS margin, Cretaceous
0.6
0.4
0.2
0.0
-0.2
-0.4
-0.6
-0.6
-0.4
-0.2
0.0
0.2
0.4

Figure 11

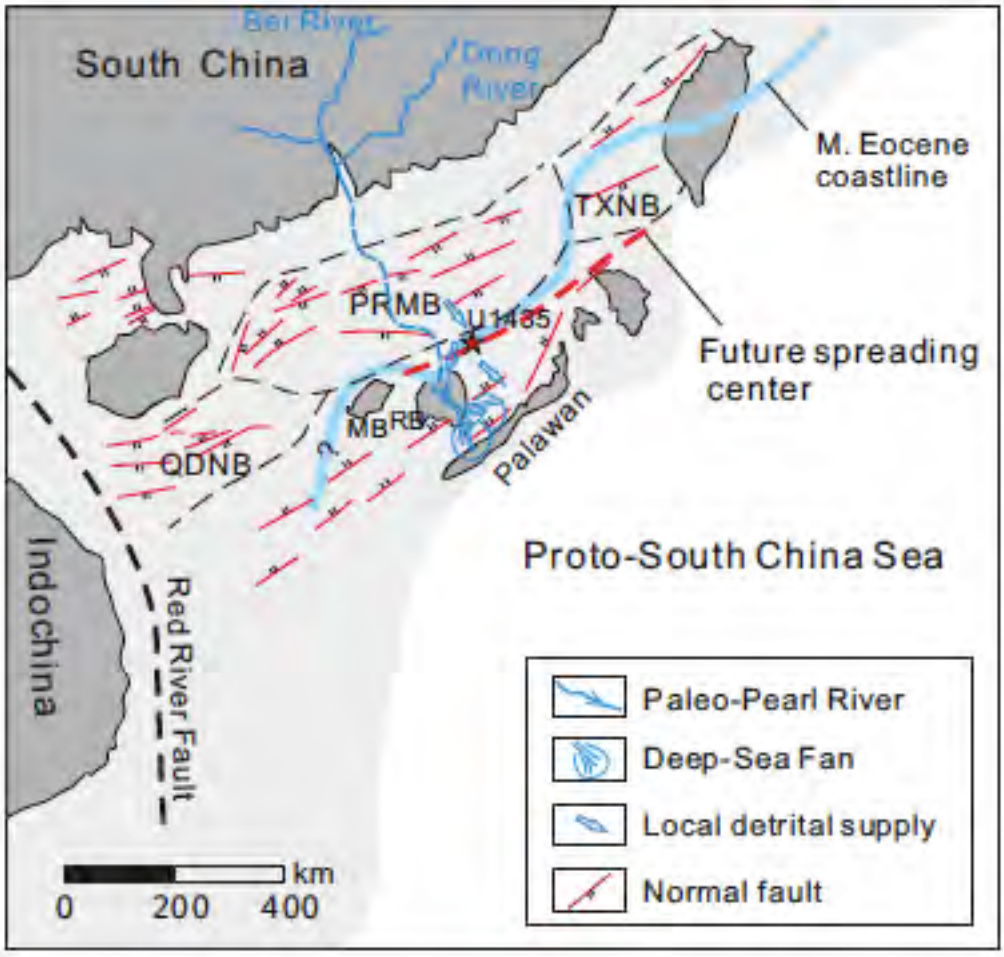
South China
Dong River
M. Eocene coastline
TXNB
PRMB
U1435
Future spreading center
MBRB
QDNB
Palawan
Proto-South China Sea
Indochina
Red River Fault
km
0
200
400
Paleo-Pearl River
Deep-Sea Fan
Local detrital supply
Normal fault

Figure 12